

POTENTIAL OF SILANES FOR CHROMATE REPLACEMENT IN METAL FINISHING INDUSTRIES

Wim J. van Ooij*, Danqing Zhu, Vignesh Palanivel, J. Anna Lamar and Matthew Stacy

Department of Materials Science and Engineering

University of Cincinnati, Ohio 45221-0012

* Corresponding author

Phone: 513-556-3194

Fax: 513-556-3773

Email: vanooijwj@email.uc.edu

Submitted to

SILICON CHEMISTRY

September 16, 2002

| Report Documentation Page | | | | Form Approved OMB No. 0704-0188 | |
|--|------------------------------------|-------------------------------------|---|---|---------------------------------|
| Public reporting burden for the collection of information is estimated to average 1 hour per response, including the time for reviewing instructions, searching existing data sources, gathering and maintaining the data needed, and completing and reviewing the collection of information. Send comments regarding this burden estimate or any other aspect of this collection of information, including suggestions for reducing this burden, to Washington Headquarters Services, Directorate for Information Operations and Reports, 1215 Jefferson Davis Highway, Suite 1204, Arlington VA 22202-4302. Respondents should be aware that notwithstanding any other provision of law, no person shall be subject to a penalty for failing to comply with a collection of information if it does not display a currently valid OMB control number. | | | | | |
| 1. REPORT DATE 16 SEP 2002 | | 2. REPORT TYPE | | 3. DATES COVERED 00-00-2002 to 00-00-2002 | |
| 4. TITLE AND SUBTITLE Potential of Silanes for Chromate Replacement in Metal Finishing Industries | | | | 5a. CONTRACT NUMBER | |
| | | | | 5b. GRANT NUMBER | |
| | | | | 5c. PROGRAM ELEMENT NUMBER | |
| 6. AUTHOR(S) | | | | 5d. PROJECT NUMBER | |
| | | | | 5e. TASK NUMBER | |
| | | | | 5f. WORK UNIT NUMBER | |
| 7. PERFORMING ORGANIZATION NAME(S) AND ADDRESS(ES) University of Cincinnati ,Department of Materials Science and Engineering,Cincinnati,OH,45221-0012 | | | | 8. PERFORMING ORGANIZATION REPORT NUMBER | |
| 9. SPONSORING/MONITORING AGENCY NAME(S) AND ADDRESS(ES) | | | | 10. SPONSOR/MONITOR'S ACRONYM(S) | |
| | | | | 11. SPONSOR/MONITOR'S REPORT NUMBER(S) | |
| 12. DISTRIBUTION/AVAILABILITY STATEMENT Approved for public release; distribution unlimited | | | | | |
| 13. SUPPLEMENTARY NOTES | | | | | |
| 14. ABSTRACT | | | | | |
| 15. SUBJECT TERMS | | | | | |
| 16. SECURITY CLASSIFICATION OF: | | | 17. LIMITATION OF ABSTRACT Same as Report (SAR) | 18. NUMBER OF PAGES 45 | 19a. NAME OF RESPONSIBLE PERSON |
| a. REPORT unclassified | b. ABSTRACT unclassified | c. THIS PAGE unclassified | | | |

POTENTIAL OF SILANES FOR CHROMATE REPLACEMENT IN METAL FINISHING INDUSTRIES

Wim J. van Ooij, Danqing Zhu, Vignesh Palanivel, J. Anna Lamar and Matthew Stacy

Department of Materials Science and Engineering, University of Cincinnati, Ohio 45221-0012

Abstract

Trialkoxysilanes (or silanes) have emerged as a very promising alternative for chromates in metal finishing industries. Compared to the conventional chromating processes, the major merits of silane-based surface treatments include: eco-compliance, easy-control processing, comparable corrosion protection of metals as well as paint adhesion to a variety of topcoats. In this overview paper, we will report the recent status of silane studies including results of corrosion performance tests, mechanism of corrosion protection of metals by silanes and thermal stabilities of silane films. We will also address the new fields that we are beginning to explore such as nano-structured silane films, “self-healing” silanes, “super-primers” and methods for in-line detection of silane films.

1. Introduction

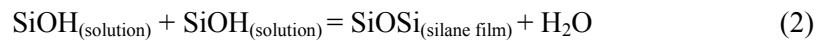
Chromates, the most efficient within the current repertoire of inhibitors, are now facing to be terminated in the field of corrosion control due to the toxic and carcinogenic nature of hexavalent chromium Cr(VI). For this reason, a number of promising candidates, so called “green inhibitors”, have been explored, with the hope of replacing chromates. Among them, silanes, a group of silicon-based organic-inorganic chemicals, have emerged as a very promising alternative. The studies associated with the corrosion protection of metals by silanes have been carried out extensively since early 1990s’ [1-16].

Trialkoxysilanes (or silanes), with the general formula of $R'(CH_2)_nSi(OR)_3$ (where R' = organic functionality; and OR = hydrolyzable alkoxy group, e.g., methoxy (OCH_3) or ethoxy (OC_2H_5)), have originally been used as effective coupling agents or adhesion promoters in glass/mineral-reinforced polymeric composites for decades [17-19]. A small amount of silanes offers a great enhancement in adhesion of polymeric matrices to inorganic reinforcements. As a result, the mechanical properties of the composites are improved dramatically.

Silanes are normally stored in the non-hydrolyzed state, and in most cases need to be hydrolyzed in their diluted aqueous solutions before application. The silane solutions become “workable” once a sufficient number of silanols ($SiOH$) are generated. In the process of silane surface treatment of metals, silane solutions can be applied onto metal surfaces by dipping, spraying and wiping. It is generally assumed that upon drying the silane-treated metals, there are two key condensation reactions occurring. One is the condensation between silanols ($SiOH$) from the silane solution and the metal hydroxyls ($MeOH$) from the metal surface hydroxides, forming covalent metallo-siloxane bonds ($MeOSi$) [17] according to,



The other is the condensation among the excess $SiOH$ groups adsorbed on the metals, forming a siloxane ($SiOSi$) film on the top:



This simplified schematic bonding mechanism is illustrated in Figure 1. Before condensation (Figure 1(a)), silane molecules are adsorbed onto the metal surface through hydrogen bonds formed between $SiOH$ groups of the silane molecules and $MeOH$ groups of the metal hydroxides. After condensation upon drying (Figure 1(b)), both $MeOSi$ and $SiOSi$ covalent

bonds are formed at the interface, giving an excellent adhesion to the metal substrate, as well as a hydrophobic interface.

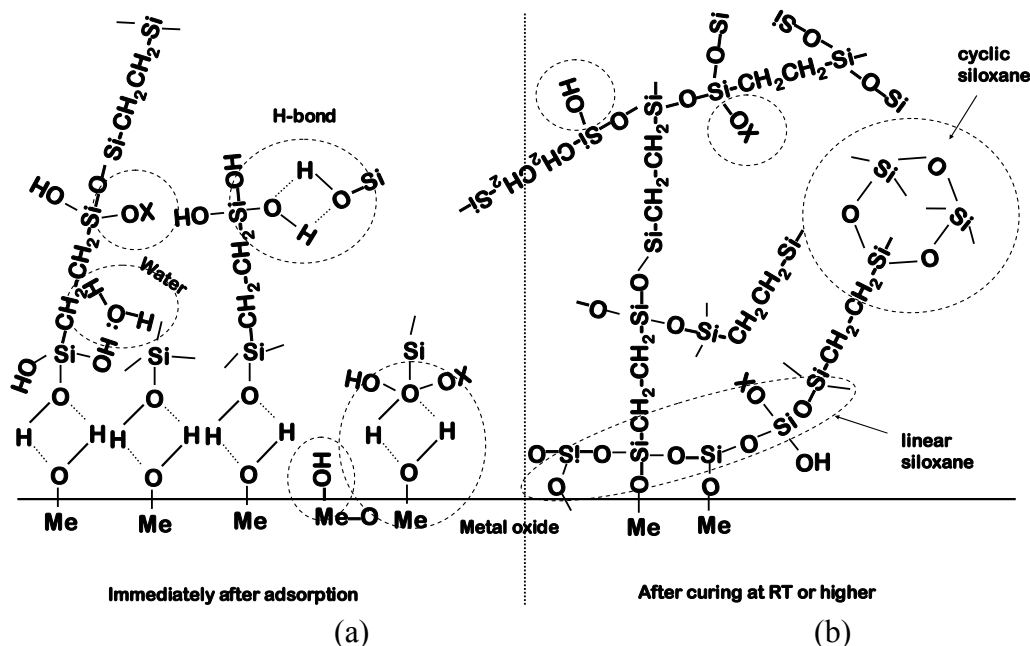


Figure 1. Simplified schematic of bonding mechanism between silane molecules and metal surface hydroxide layer; (a) before condensation: hydrogen-bonded interface; and (b) after condensation: covalent-bonded interface [20]

In light of their chemical structures, the silanes suitable for corrosion protection can be divided into two major categories, i.e., “mono-silanes” and “bis-silanes”. Mono-silanes are the silane coupling agents mentioned above, examples of which are vinyltriethoxysilane (VS, $\text{CH}_2\text{CHSi}(\text{OC}_2\text{H}_5)_3$) and γ -ureidopropyltriethoxysilane (γ -UPS, $\text{H}_2\text{NCONH}(\text{CH}_2)_3\text{Si}(\text{OC}_2\text{H}_5)_3$). Bis-silanes, with the general formula of $(\text{OR})_3\text{Si}(\text{CH}_2)_n\text{R}'(\text{CH}_2)_n\text{Si}(\text{OR})_3$, are mainly used as crosslinkers for silane coupling agents [17]. Examples of bis-silanes are bis-[3-(triethoxysilylpropyl)]ethane (BTSE, $(\text{OC}_2\text{H}_5)_3\text{Si}(\text{CH}_2)_2\text{Si}(\text{OC}_2\text{H}_5)_3$), bis-[3-(triethoxysilyl)propyl]tetrasulfide (bis-sulfur silane, $(\text{OC}_2\text{H}_5)_3\text{Si}(\text{CH}_2)_3\text{S}_4(\text{CH}_2)_3\text{Si}(\text{OC}_2\text{H}_5)_3$), bis-

[3-(trimethoxysilylpropyl)]amine (bis-amino silane, $(\text{OCH}_3)_3\text{Si}(\text{CH}_2)_3\text{NH}(\text{CH}_2)_3\text{Si}(\text{OCH}_3)_3$) and their mixtures. The major difference between mono- and bis-silanes is that the number of hydrolyzable OR groups in a bis-silane molecule is double that in a mono-silane molecule, as illustrated in Figure 2. A mono-silane molecule only has 3 OR groups attached to the silicon (Si) atom at one end (Figure 2(a)); while a bis-silane molecule has 6 OR groups in total and 2 Si atoms at both ends, with every 3 OR groups attached to a Si atom (Figure 2(b)). It has consistently been observed in corrosion performance tests that the bis-silanes offer a much better corrosion protection with and without topcoats than the mono-silanes to various metals and alloys, such as steels, Al and Al alloys, Zn and Zn-coated steels, Cu and Cu alloys, and Mg and Mg alloys [1-16]. It is believed that the stronger interfacial adhesion and denser films of bis-silanes is one of the key factors that contribute to their much better corrosion performance on metals, as compared to mono-silanes, especially in unpainted state.

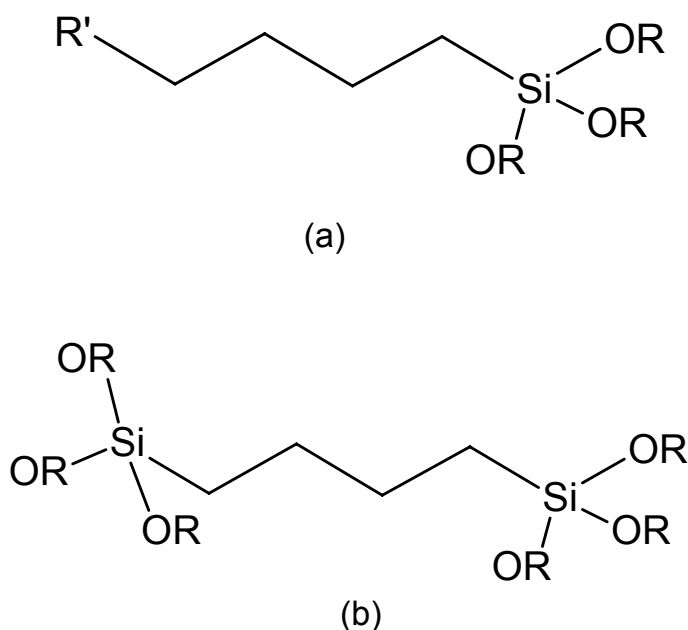
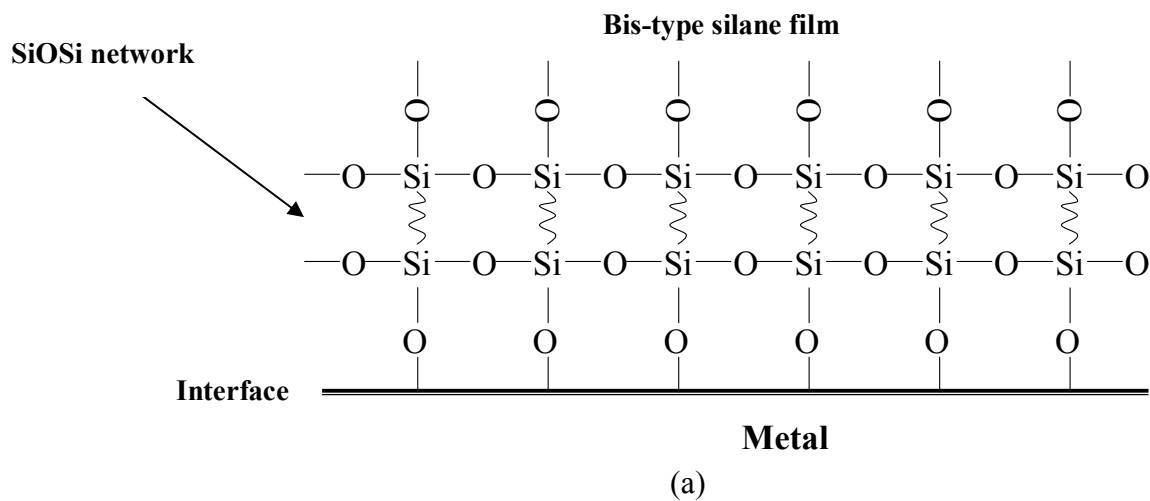


Figure 2. Structures of bis-silane molecule (a), and mono-silane molecule (b) [20]

As shown in Figure 2, each bis-silane molecule contains 6 hydrolyzable OR groups, which doubles the number of that of mono-silane molecule. Assuming that both silanes are hydrolyzed completely in their solutions, then each bis-silane molecule would generate 6 SiOH groups available for the subsequent condensation reactions while each mono-silane molecule only has 3 SiOH groups. As a result, bis-silane molecules are capable of reacting with the metal substrate forming an interface with a high density of MeOSi bonds and in the meantime building up a crosslinked silane film (i.e., SiOSi network) of an appreciable thickness, as shown in Figure 3(a) [20]. Mono-silane molecules, however, cannot achieve this. Figure 3(b) shows a possible interfacial region developed in the mono-silane system. Apparently, the structure is much more porous than the bis-silane system, due to the lack of sufficient amount of SiOH groups. On the basis of this comparison, it is reasonable to expect that the bis-silanes have a stronger adhesion to the metal substrate than the mono-silanes, and more resistance to water diffusion as SiOSi units are hydrophobic, as opposed to SiOH groups which are hydrophilic.



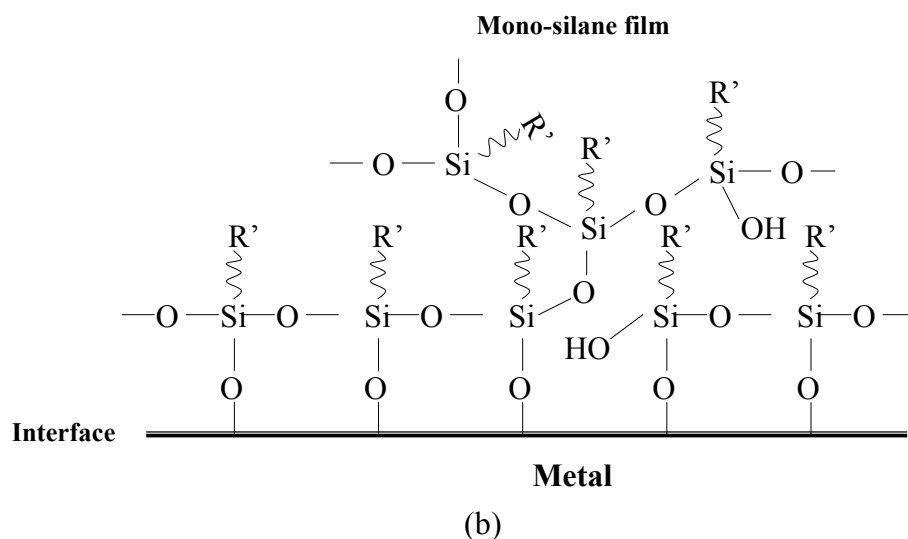


Figure 3. Bonding mechanism in mono-type silane/metal system; (a) bonding of bis-silane to metal; and (b) bonding of mono-silane to metal [20]

Another group of silanes, i.e., water-based silanes or silane mixtures, have also been studied in our laboratory. This effort is mostly as a response to the call for a reduction of Volatile Organic Compounds (VOC) in metal-finishing industries. The major merit of these water-based silanes is that only de-ionized (DI) water is needed for silane solution preparation. The silane hydrolysis in the silane solutions is instantaneous. A good representative for these water-soluble silanes is the mixtures of bis-amino silane and vinyltriethoxysilane (VTAS), some test results for which are presented later in this paper.

Regardless the silane type, the silane film thickness is always linearly proportional to the corresponding silane solution concentrations, as shown in Figure 4 [4,21]. It is clearly seen that the film thicknesses of all three silane films, i.e., bis-amino silane, bis-sulfur silane, and the silane mixture of bis-amino silane and VTAS (or bis-amino/VTAS mixture) are well-determined by their silane solution concentrations. The water-based bis-amino/VTAS silane film, in general, is thinner than those two solvent-based silane films. This finding supports the conclusion that silane

film thickness can be mainly controlled by adjusting the corresponding silane solution concentration.

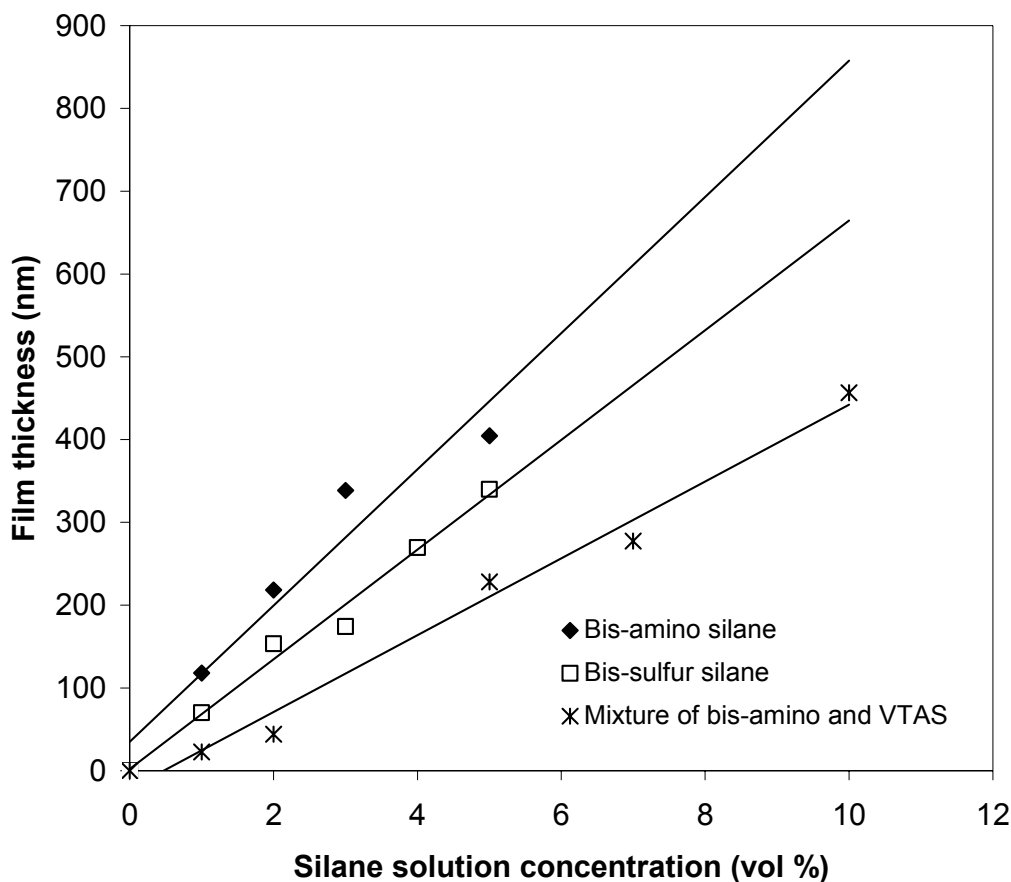


Figure 4. Film thicknesses of silanes as a function of silane solution concentration [4,21]

It was confirmed in our previous works that SiOH groups cannot be condensed to form a solid siloxane (SiOSi) film on metal surfaces in aqueous media. Therefore, silanes are not considered as a solution phase corrosion inhibitor as chromates do. Since silane films are only formed upon drying via condensation reactions (1) and (2), contact time or dipping time of metals in silane solutions thus does not have any noticeable effect on the formation of silane films. Our previous work also showed that the obtained film thickness was independent of contact time [12].

This is different from a conventional chromating process, where a chromate layer is deposited onto a metal in the immersion step and the film thickness is determined by the contact time.

It also should be pointed out that the performance of silanes is dependent on the type of metals. In many cases, different metals may require different silanes. On the basis of our previous works, Table 1 summarizes the silanes and the corresponding metals which can be protected by these silanes. This information can serve as a brief guide for silane selection for the purpose of corrosion protection of metals.

Table 1. A brief guide of corrosion protection of metals by silanes

| Silane | Metals protected |
|--|---|
| Bis-[3-(triethoxysilyl)propyl]-tetrasulfide (bis-sulfur silane) | Al and Al alloys, steels, |
| Mixtures of bis-[3-(trimethoxysilyl-propyl)]amine and bis-[3-(triethoxysilyl-propyl)-tetrasulfide (mixtures of bis-sulfur and bis-amino silanes) | Al and Al alloys, steels, Zn and Zn-coated steels, Cu and Cu alloys, Mg and Mg alloys |
| Bis-[3-(triethoxysilylpropyl)]ethane (BTSE) | Al and Al alloys, steels |
| Mixtures of bis-[3-(trimethoxysilyl-propyl)]amine and vinyltriethoxysilane (mixtures of bis-amino and VTAS) | Al and Al alloys, steels, Zn and Zn-coated carbon steels, stainless steels and CrCo alloy |

2. Experimental

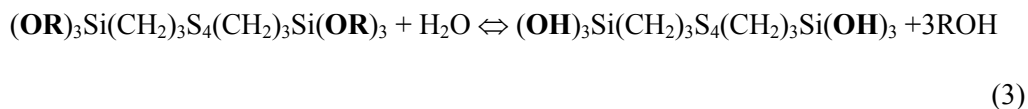
2.1. Silanes

Bis-[3-(triethoxysilyl)-propyl]tetrasulfide (or bis-sulfur silane) and bis-[3-(trimethoxysilyl)propyl]amine (bis-amine silane), with the trade names of Silquest A1289[®] and Silquest A1170[®], respectively, were provided by OSi Specialties (Tarrytown, NY). Bis-[trialkoxysilyl]alkane silanes, i.e., bis-[trimethoxysilyl]methane (BTSM), bis-[triethoxysilyl]ethane (BTSE), bis-[trimethoxysilyl]hexane (BTSH), and bis-[triethoxysilyl]octane (BTSO) were also provided by OSi Specialties. Vinyltriethoxysilane (VTAS) was purchased from Gelest Inc. (Tullytown, PA). Table 2 gives the chemical structures of these silanes. The silanes were used without further purification. Their purity was reported > 95%.

Before application, the hydrolysable OR groups of these silanes need to be converted to active SiOH groups in their diluted aqueous solutions for the subsequent condensation reactions mentioned above. A 5 vol.% bis-sulfur silane solution, for example, was prepared by adding the silane to a mixture of DI water and ethanol. The ratio of bis-sulfur silane/DI water/ethanol was 5/5/90 (v/v/v). The natural pH of the solution was 6.5. The solution was stirred for 10 minutes, and then aged in ambient conditions for at least 2 days to ensure that the solution became “workable” [16]. In other words, although complete hydrolysis is not necessary, a sufficient number of active SiOH groups should be generated in the solution for the condensation reactions (1) and (2) listed earlier. In this way, a solid rather than an oily silane film is formed on metal substrates. The hydrolysis reaction equilibrium in the bis-sulfur silane solution is given by

Table 2. Chemical structures of silanes used in this work

| Silane Name | Molecular Structure |
|--|---------------------|
| Bis-[3-(triethoxysilyl)propyl]-tetrasulfide (bis-sulfur silane) $(\text{OC}_2\text{H}_5)_3\text{Si}(\text{CH}_2)_3\text{S}_4(\text{CH}_2)_3\text{Si}(\text{OC}_2\text{H}_5)_3$ | |
| Bis-[3-(trimethoxysilyl)propyl]amine (bis-amino silane) $(\text{OCH}_3)_3\text{Si}(\text{CH}_2)_3\text{NH}(\text{CH}_2)_3\text{Si}(\text{OCH}_3)_3$ | |
| Vinyltriacetoxysilane (VTAS) $\text{CH}_2=\text{CH}(\text{CH}_2)_2\text{Si}(\text{OCOCH}_3)_3$ | |
| Bis-[3-(triethoxysilyl)propyl]methane (BTSM) $(\text{OC}_2\text{H}_5)_3\text{Si}(\text{CH}_2)\text{Si}(\text{OC}_2\text{H}_5)_3$ | |
| Bis-[3-(triethoxysilyl)propyl]ethane (BTSE) $(\text{OC}_2\text{H}_5)_3\text{Si}(\text{CH}_2)_2\text{Si}(\text{OC}_2\text{H}_5)_3$ | |
| Bis-[3-(triethoxysilyl)propyl]hexane (BTSH) $(\text{OC}_2\text{H}_5)_3\text{Si}(\text{CH}_2)_6\text{Si}(\text{OC}_2\text{H}_5)_3$ | |
| Bis-[3-(triethoxysilyl)propyl]octane (BTSO) $(\text{OC}_2\text{H}_5)_3\text{Si}(\text{CH}_2)_8\text{Si}(\text{OC}_2\text{H}_5)_3$ | |



where the subscript 4 is the average number of the S atoms contained in each bis-sulfur silane molecule; OR = hydrolyzable alkoxy groups or OC₂H₅ in the case of the bis-sulfur silane. It should be noted that this reaction occurs in steps [22] and it is not possible to approach completion if ethanol is the solvent for the silane solution [6].

Bis-amino/VTAS silane mixtures are water soluble. The solution preparation is therefore relatively simple. A 5% bis-amino/VTAS silane mixture at the ratio of 1/1, for example, is simply prepared by mixing the two silanes together, and then adding 5 parts of the silane mixture into 95 parts of DI water. The solution was stirred for a few seconds until it became clear.

2.2. Silane surface treatment

The metal panels to be treated were degreased in a diluted alkaline cleaner (AC1055[®], provided by Brent America Inc., Lake Bluff, IL) at 65 °C for 3-5 min, rinsed with tapwater, and then dried with compressed air. The cleaned panel surfaces should be completely “water-break-free” (i.e., thoroughly wettable by water). The cleaned panels were dipped into the silane solutions 1-5 s, and then dried in air at either room temperature or an elevated temperature (e.g., 100°C for 10 min), in order to drive the solvents (water and/or organic solvents) out of the films and to make the silane films crosslinked. The crosslinked silane structure is extremely stable and does not dissolve in water or most organic solvents such as ethanol [21].

2.3 Characterization techniques

Two major film characterization techniques are Fourier-Transform Infrared Reflection-Absorption (FTIR-RA) spectroscopy and Electrochemical Impedance Spectroscopy (EIS). They were employed extensively for silane film characterization. The FTIR technique is a powerful

tool in the field of polymer characterization, while the capability of EIS as a thin film characterization technique had not been demonstrated until recently [6,16]. EIS has for a long time been used as one of the most valuable techniques in corrosion field for monitoring the performance degradation of polymeric coatings on metals when exposed to corrosive aqueous environments (e.g., NaCl solution) [23-26].

FTIR-RA measurements were conducted on a Bio-Rad FTS-40 spectrophotometer in the mid-IR range from 4000 to 400 cm^{-1} . All spectra were obtained at an incident angle of 75° normal to the surfaces of the specimens, with a spectral resolution of 4 cm^{-1} and the number of scans was 100.

EIS measurements on silane-coated metals (mainly on AA 2024-T3) were carried out in a 0.5 M K_2SO_4 neutral aqueous solution (non-corrosive to Al alloys), using an SR 810 frequency response analyzer and a Gamry CMS 100 potentiostat. Impedance data were recorded at frequencies ranging from 10^{-2} to 10^5 Hz, with the alternating current (AC) voltage amplitude of ± 10 mV. A commercial Saturated Calomel Electrode (SCE) served as the reference electrode, coupled with a graphite counter electrode. An area of 3.14 cm^2 of the specimen was exposed to the electrolyte during the measurements. The reason for using the noncorrosive electrolyte K_2SO_4 here was to avoid possible corrosion activity at the metal substrate during the measurements, since the corrosion information included in the EIS plots would lead to the data interpretation being unnecessarily complicated.

2.4 Corrosion tests

DC polarization tests were carried out on AA 2024-T3 panels with and without silane treatments in a naturally aerated 0.6 M NaCl solution at pH 6.5. The silane-treated panels were pre-immersed in the electrolyte for 5 hours before data acquisition. The reason for pre-immersing the silane-treated panels was to allow the silane film being saturated with the electrolyte before

testing. Therefore, the DC data collected afterwards can be considered as a reflection of the corrosion performance of the entire system of silane film and the metal/silane interface rather than just that of the surface of silane films. The bare AA 2024-T3 panels were tested immediately after exposure to the electrolyte. An SCE and a platinum mesh were used as the reference and counter electrodes, respectively. The exposed area was 0.78 cm^2 . On the average, 5 replicate samples were tested for each condition. The data were recorded over the range of $E_{\text{corr}} - 0.25 \text{ V/SCE}$ to $E_{\text{corr}} + 0.25 \text{ V/SCE}$ (where, E_{corr} is corrosion potential of the tested samples). The scan rate was 1 mV/s .

EIS measurements were employed to monitor the corrosion performance of the silane-treated AA 2024-T3 system as a function of immersion time in a 0.6 M NaCl solution ($\text{pH } 6.5$). The other experimental parameters were the same as described in Section 2.3, except for the electrolyte. Instead of noncorrosive K_2SO_4 , a neutral 0.6 M NaCl aqueous solution (corrosive to most metals) was used here.

ASTM B117 (Salt spray test, SST) This test was employed to evaluate bare corrosion protection of silane-treated metals without topcoats. According to the specification, a 5% salt solution (NaCl) is atomized in a salt spray chamber at 35°C with the solution pH around 7. The tested panels is placed at an angle of 45° in the chamber, exposing to the salt fog for a certain period [27].

ASTM 1654-92 (Corrosion test for painted or coated metals and alloys) This test provides a method to evaluate the corrosion performance and paint adhesion of painted alloys with silane pretreatment. The testing conditions are similar to that for ASTM B117, except that the painted metal surfaces need to be scribed prior to salt spray testing. Delamination area is measured along the scribe line after exposure, the value of which is often used as a measure for the corrosion performance and paint adhesion of the painted systems [27].

ASTM B368 (Copper-accelerated acetic acid-salt spray testing, CASST) This test is derived from ASTM B117. 0.25 g/liter copper chloride ($\text{CuCl}_2 \bullet 2\text{H}_2\text{O}$) is added into 5% NaCl

solution. The pH of the salt copper solution shall be adjusted to the range of 3.0 to 3.3 by the addition of glacial acetic acid. The temperature in a salt spray chamber is 49°C [27].

3. Results of Corrosion Performance tests

3.1. *Bare corrosion protection of metals by silane surface treatments (without paints)*

Silane-treated AA 7075-T6 panels after 336 hrs of salt spray exposure are shown in Figure 5, along with chromated (using an Alodine standard process) and bare panels as controls. Prior to the test, The AA 7075-T6 panels were treated with a 5% bis-sulfur solution, and then cured at 100°C for 10 min. It is clearly seen that both silane-treated and chromated surfaces do not exhibit any sign of corrosion. The silane-treated panel still retains its originally shiny surface. The chromated panel, although no gross corrosion is visible, show some discoloration. The bare panels, in contrast, exhibit severe corrosion after only 20 hrs of exposure. A 336-hr salt spray test was also conducted on bis-sulfur silane-treated AA 2024-T3 and AA 6061-T6 panels, and the same trend was seen in the results after exposure. Nevertheless, it should be pointed out that the bis-sulfur silane film obtained from a 5% silane solution is about 400 nm thick; while the chromate has a typical thickness of greater than 1000 nm. Thus, silane films outperform chromate films on a per-weight basis.

The results shown in Figure 6 are AA 5005 panels subjected to different pre-treatments, and then exposed to a salt spray for 29 days. The untreated panel has corroded thoroughly after testing; the chromated surface shows severe discoloration and a small number of tiny pits. The bis-amino/VTAS silane mixture treated panels, on the contrary, does not show any corrosion on the surface.

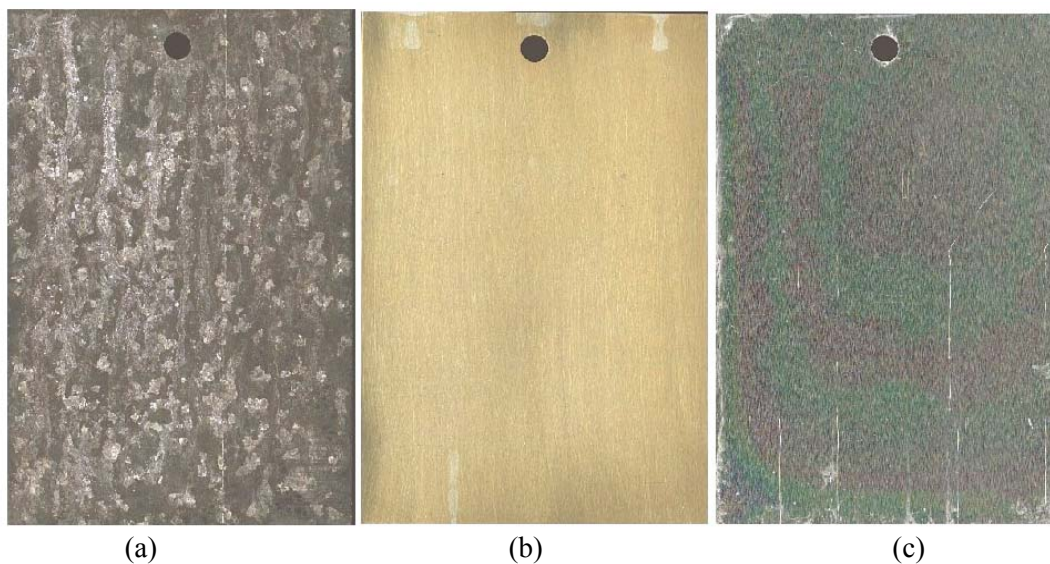


Figure 5. AA 7075-T6 after 336 hrs of salt spray testing; (a) Untreated (20 hrs of testing), (b) chromated (Alodine[®] product), and (c) Bis-sulfur silane treated (5%, pH 6.5)

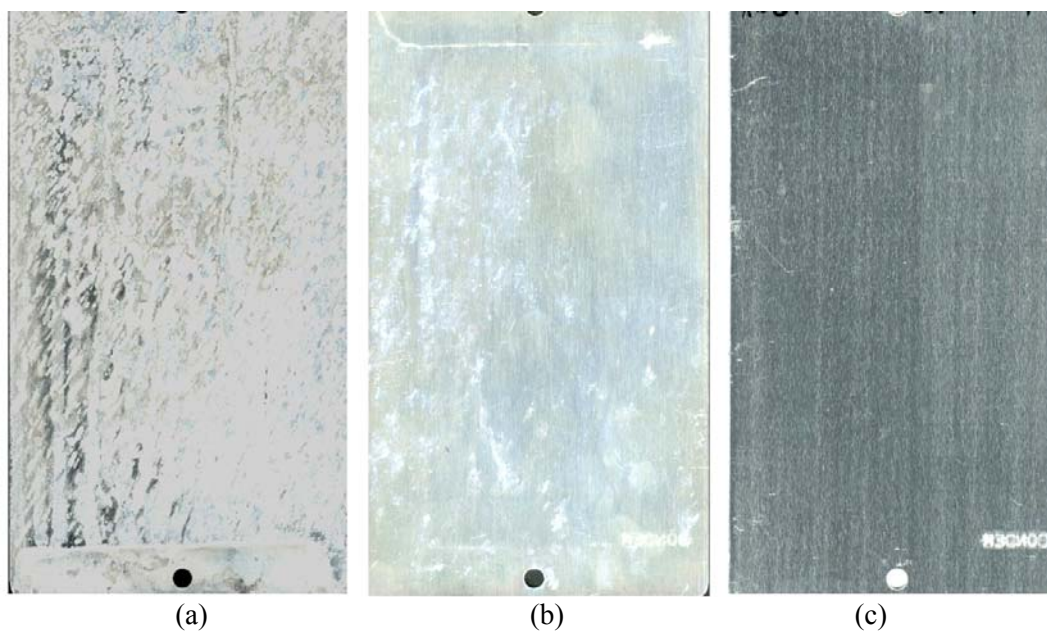


Figure 6. AA 5005 panels after 29 days of salt spray testing, (a) untreated, (b) chromated (chromicoat 103[®]), (c) silane-treated (5%, bis-amino/VTAS, 1/1, pH 4)

It was noted that the bis-sulfur silane always provide good corrosion protection on a variety of Al alloys, but it totally fails when used on hot-dip galvanized steel (HDG) if used without further paints. A recent study showed that if bis-sulfur and bis-amino silanes are mixed at a certain ratio, e.g., 3/1, this mixture improves the corrosion performance of both HDG and AA 2024-T3 significantly. Figure 7 shows a 8-day neutral NaCl immersion test result of the HDG panels subjected to different silane treatments. It is clearly seen that both bis-sulfur and bis-amino silane treated HDG corroded heavily in the immersion, but the bis-sulfur/amino silane mixture treated HDG surface remains intact. Understanding of this unique behavior of the mixture is one of our current research subjects, and details will be published elsewhere.

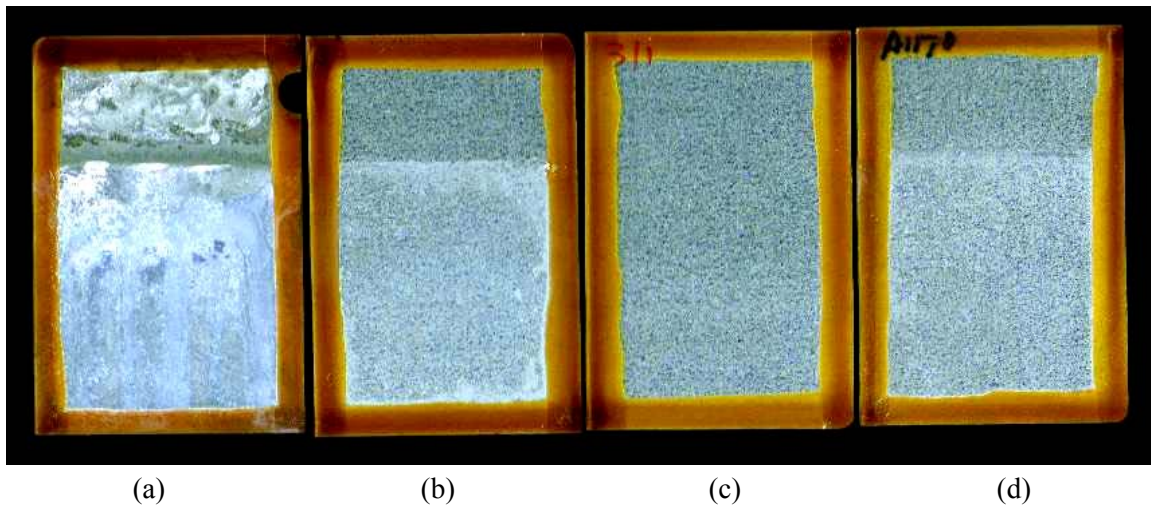


Figure 7. HDG panels after 8 days of immersion in 0.6M NaCl solution; (a) Untreated, (b) Bis-sulfur silane treated (5%, pH 6.5), (c) Bis-sulfur/amino silane treated (5%, bis-sulfur/amino=3/1, pH 7.0), and (d) Bis-amino silane treated (5%, pH 7.0)

3.2. Improved corrosion protection of painted metals by silane pretreatment

All silanes investigated here can be applied on a wide range of metals for the purpose of paint adhesion improvement as well as corrosion protection. The paints commonly tested in our work include: epoxies, polyurethanes, polyesters, acrylics and rosin-based paints.

Figure 8 shows polyurethane powder-painted AA 2024-T3 panels after 1008 hours of salt spray test (ASTM B117). The panel without any pretreatment exhibits a large extent of paint delamination after testing, while the chromated and the silane treated panels do not exhibit any paint delamination along the scribe lines.

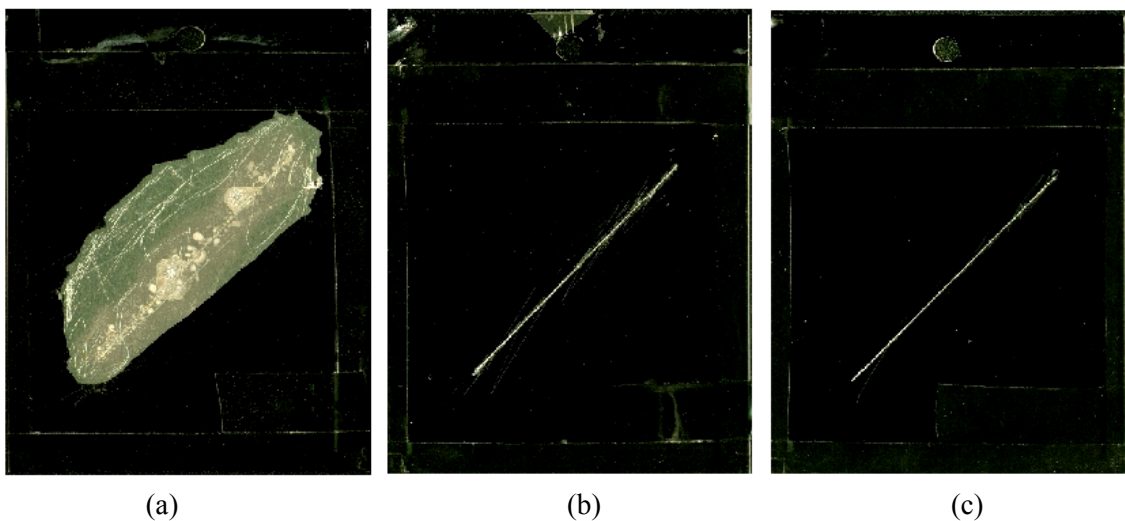


Figure 8. Polyurethane powder painted AA 2024-T3 after 1008 hrs of SST, (a) untreated, (b) chromated (CHEM-CODE 105[®]), and (c) silane-treated (2%, bis-amino/VTAS=1.5/1, pH 4)

Water-based bis-amino/VTAS silane pre-treated AA 5005 panel after painted with polyester powder paint was also tested for 240 hrs in the copper-accelerated acetic acid salt spray test (ASTM B368). The result is shown in Figure 9. The control systems used here were untreated and chromated panels. It is seen that the untreated shows a severe paint delamination and a heavy corrosion underneath; whereas both chromated and silane-treated panels survive very well without showing any paint delamination.

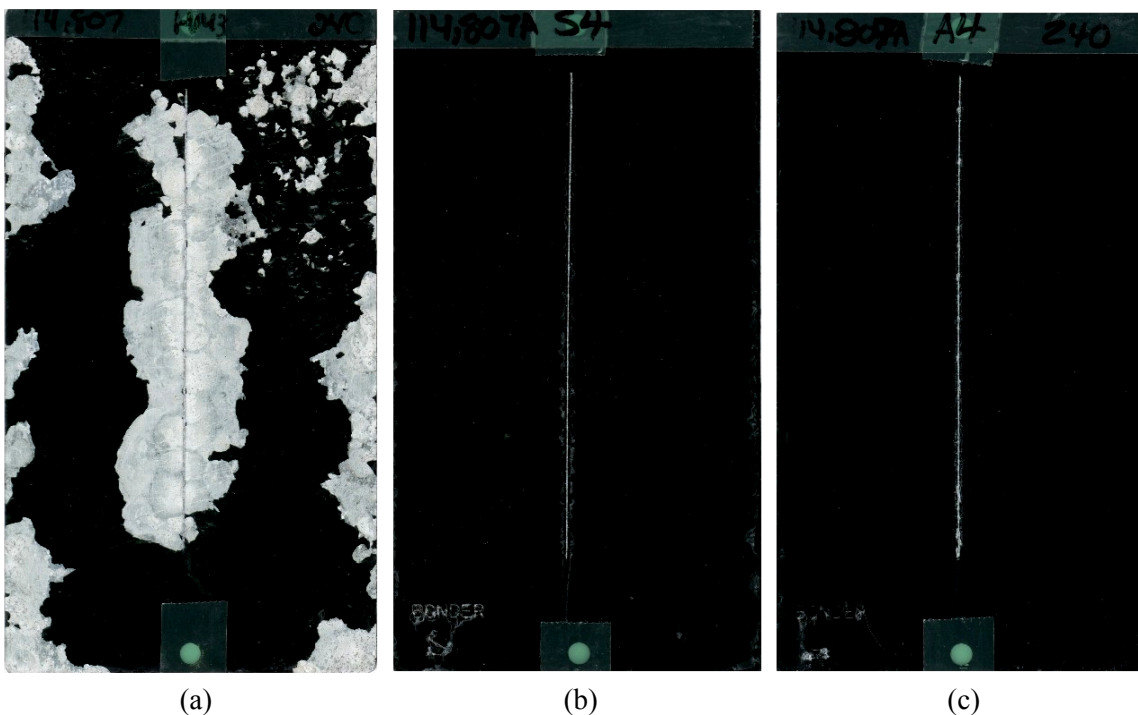


Figure 9. Polyester powder painted AA 5005 panels after 240 hrs of CASST, (a) Untreated, (b) Chromated (CHEM-CODE 105[®]), and (c) Silane-treated (2%, bis-amino/VTAS=1.5/1, pH 4)

4. Mechanisms

4.1. Characterization of silane films on metals using FTIR-RA and EIS

Bis-sulfur and bis-amino silanes were characterized extensively using FTIR-RA and EIS, in order to clarify the following important effects on the structures of silane films.

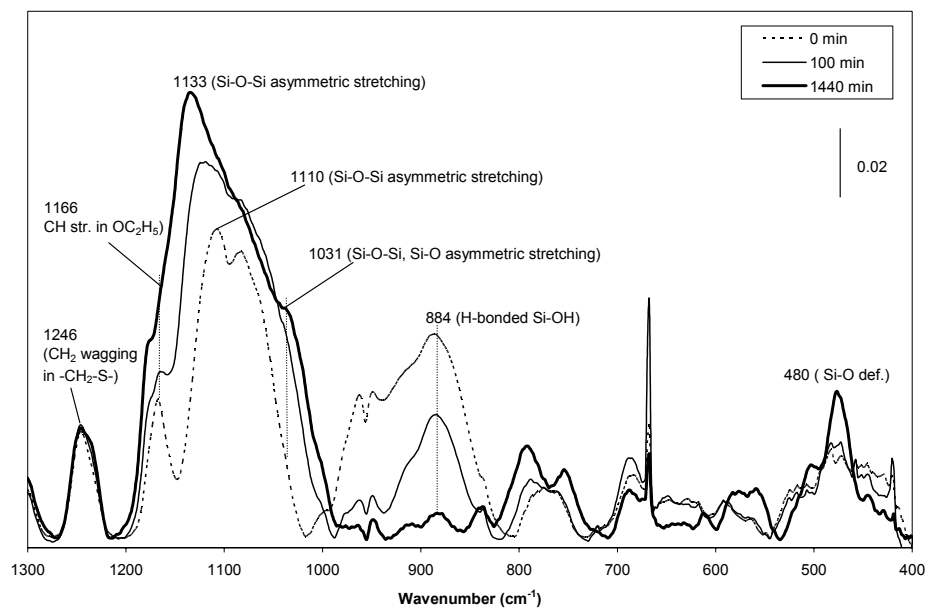
Hydrolysis time of silane solutions. Hydrolysis time of silane solutions is a very important parameter in silane surface treatment. The silane solution cannot generate enough SiOH groups without sufficient hydrolysis time. An oily and less-crosslinked silane film is often obtained from a poorly hydrolyzed silane solution due to the lack of a sufficient number of SiOH groups generated in the solution. Such an oily silane film is not expected to offer good corrosion

protection to metals, since it cannot obtain a crosslinked structure and a good adhesion to metal substrates without sufficient active SiOH groups.

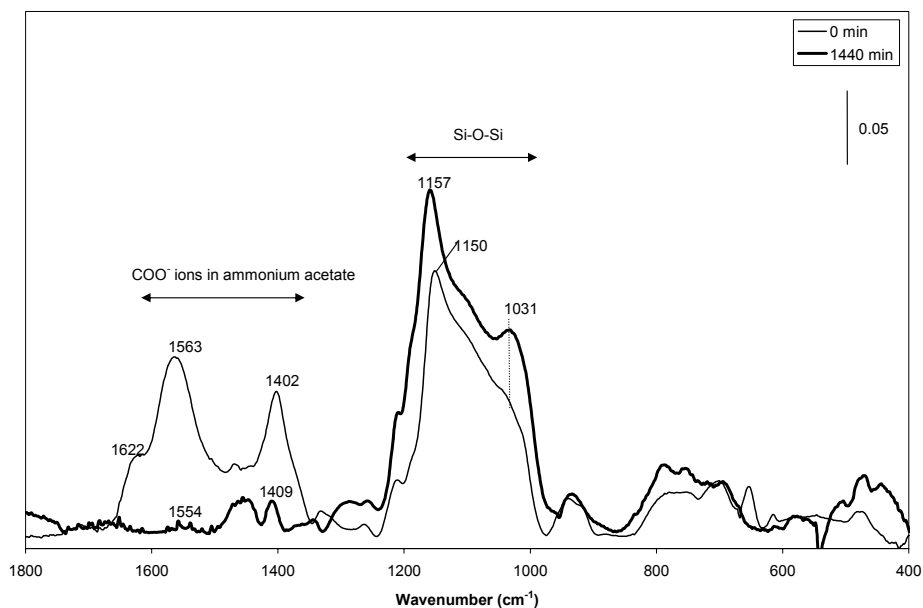
It was found [16] that in order to obtain a sufficient amount of silanols, a minimum hydrolysis time is required for both bis-sulfur and bis-amino silane water/alcohol solutions: at least 50 hrs for a 5% bis-sulfur silane solution at its natural pH (6.5); and 4 hrs for a 5% bis-amino silane solution at pH 7.5 (adjusted by acetic acid). The bis-amino silane was observed to hydrolyze much faster than the bis-sulfur silane. This is because the secondary amino groups (NH-) function as a catalyst for the silane hydrolysis. In other words, the bis-amino silane hydrolyzes by way of auto-catalytic effect.

The hydrolysis of water-based silanes is much faster and tends to completion, as compared to the above solvent-based silanes. It was observed that a bis-amino/VTAS solution, for example, is ready for use only after 5 min of mixing.

Structural changes of silane films under various curing processes. The structure of silane films experiences certain changes when curing with different conditions. Figures 10a and b show the FTIR-RA spectra of bis-sulfur and bis-amino silane films after curing at 100°C for various times. In Figure 10a, the bands centered at 1100 cm^{-1} due to SiOSi become more intensive as the curing time increases. The whole region becomes broader as compared to that without curing. In addition, the major band for SiOSi has shifted to higher frequencies from 1110 cm^{-1} at 0 min to 1133 cm^{-1} at 1440 min (24 hr). All of these changes indicate that the bis-sulfur silane film has experienced an extensive crosslinking forming a denser siloxane network during the curing period. Besides, it is also noticed that the band at 885 cm^{-1} due to hydrogen-bonded SiOH decreases in intensity with curing time, confirming that the siloxanes have formed via the consumption of the silanols. It should be noted that a similar IR change was also seen when immersing the bis-sulfur silane film deposited on AA 2024-T3 in water or simply aging at the ambient, which suggests that the crosslinking can proceed in the bis-sulfur silane film during immersion and ambient aging [6].



(a)



(b)

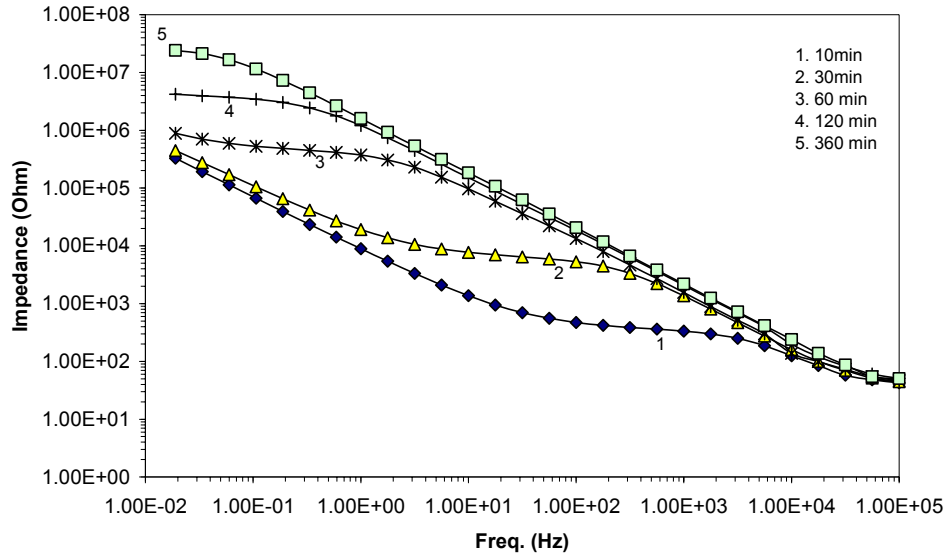
Figure 10. FTIR-RA spectra of bis-type silane films on AA 2024-T3 after curing at 100°C in air for various times; (a) bis-sulfur silane film and (b) bis-amino silane film [16]

In Figure 10b, the FTIR-RA spectra of the bis-amino silane film on AA 2024-T3 after curing at 100°C for various times are shown. The bands at 1622 cm^{-1} , 1563 cm^{-1} , and 1402 cm^{-1}

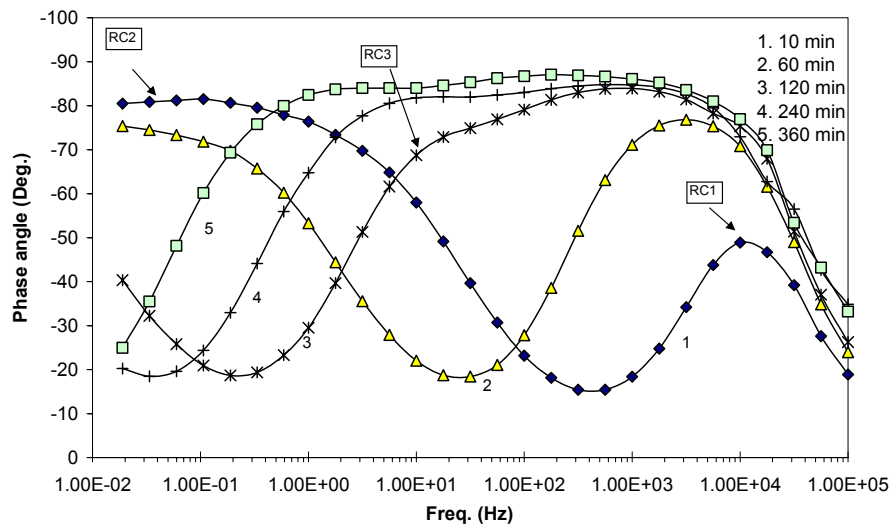
at 0 min (not cured) are due to the carboxylate ions (COO^-) in the ammonium acetate formed between the secondary amines and the acetic acid [28]. The possible form of these acetates is $-\text{NH}_2^+\text{COO}^-$. After curing at 100°C for 120 min (not shown), these acetates bands have almost diminished, indicating that the acetate in the bis-amino silane film has been removed, probably via decomposition of these compounds and followed by the evaporation from the film. The SiOSi band at 1150 cm^{-1} before curing has shifted to 1157 cm^{-1} after curing for 1440 min, along with an increase in intensity. This means that a further crosslinking has occurred in the film resulting in a denser siloxane network. The band near 880 cm^{-1} due to hydrogen-bonded SiOH , is not observed for the bis-amino silane even before curing (0 min). This implies that the SiOH groups in the bis-amino silane film have already been condensed even before curing, and further curing only results in further maturing of the siloxane network. It was also found that when ageing a bis-amino silane film in the ambient conditions, water-soluble carbamates and/or bicarbonates are formed in the film, as detected in both IR and EIS measurements [16]. This effect had been reported by others for γ -aminopropyltrimethoxysilane (γ -APS, $\text{N}_2\text{H}(\text{CH}_2)_3\text{Si}(\text{OCH}_3)_3$) [29-31].

EIS has been demonstrated to be a powerful characterization technique throughout this silane work [6,16]. EIS measurements of bis-sulfur and bis-amino silane films have been carried out in a non-corrosive electrolyte (e.g., 0.5 M neutral K_2SO_4 aqueous solution). EIS results are consistently in good agreement with the IR results. Moreover, EIS is more sensitive to the subtle structural changes in the silane/metal interfacial region than FTIR. Figure 11, for example, shows the EIS spectra (in the form of Bode plots) of bis-sulfur silane film on AA 2024-T3 after curing at 80°C for various times [6]. The impedance increases over curing time in Figure 11(a). This is, apparently, caused by the further crosslinking in the film confirmed by FTIR. In Figure 11(b), the time constant RC1 due to the silane film broadens upon curing, indicating the film experiences crosslinking. The time constant RC2 corresponding to the inner Al oxide layer shifts to lower frequencies, suggesting that the surface of the oxide layer has also been modified by the silane

deposition. The most important event shown in Figure 11(b) is the appearance of a new time constant (RC3) in the mid-frequency range upon curing. RC3 becomes obvious after 120 min of curing in Figure 11(b). This is believed to indicate the formation of a new structure formed in the interfacial region. Such interfacial information is difficult to extract from the FTIR-RA study.



(a)



(b)

Figure 11. Bode plots of bis-sulfur silane coated AA 2024-T3 after curing at 80°C in air for various times, measured in 0.5 M K₂SO₄ solution (pH 6.5); (a) impedance plot, and (b) phase angle plot [6]

On the basis of the above characterization work, a general structure model of the bis-silane treated Al system is proposed, as illustrated in Figure 12 [16]. A silane/Al system comprises three different layers. From outside to inside, they are the crosslinked silane film containing SiOSi bonds, the highly condensed interfacial layer consisting of SiOSi and SiOAl bonds, and the inner metal oxide layer. The knowledge of such film structure is very essential for further understanding the picture of corrosion control of metals by silanes.

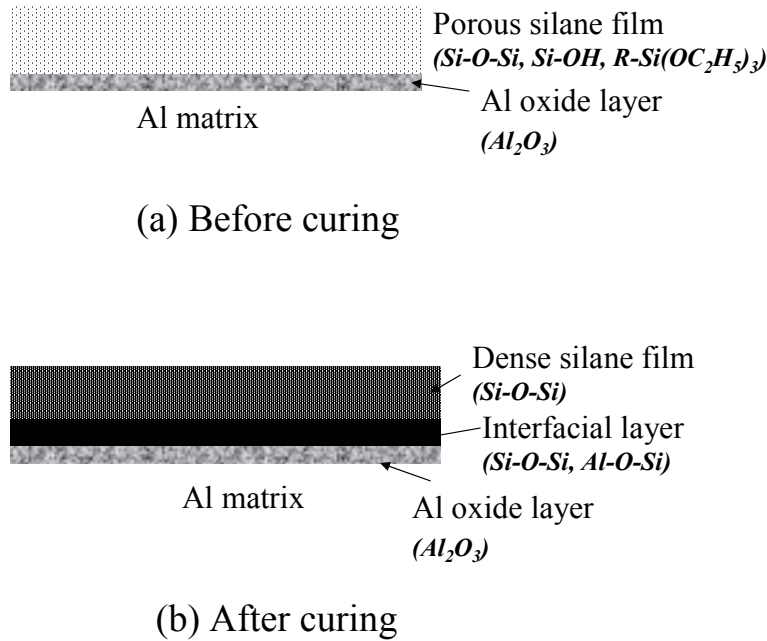


Figure 12. Schematic of structural evolution of bis-sulfur silane system upon curing; (a) before curing; and (b) after curing [16]

4.2. Corrosion study of bis-sulfur silane-treated AA 2024-T3 in neutral NaCl solution

In order to get a better insight into the corrosion protection of metals by silanes, the corrosion performance of bis-sulfur silane-treated AA 2024-T3 in neutral NaCl solution was

studied using electrochemical tests and scanning electronic microscopy (SEM) equipped with energy dispersive X-ray spectrometry (EDX) [20].

Figure 13 displays DC polarization curves of AA 2024-T3 treated with and without the bis-sulfur silane, obtained from a 0.6 M NaCl solution (pH 6.5, open to air). The bis-sulfur silane treated AA 2024-T3 panels were immersed in the electrolyte for 5 hrs before data collection for the reason mentioned earlier. In Figure 13, both anodic and cathodic current densities of AA 2024-T3 have been reduced by more than 2 decades after the silane treatment (curve 2) at the applied voltages with respect to that of the bare AA 2024-T3 (curve 1). The E_{corr} of AA 2024-T3 and the curve shapes, however, do not show a substantial variation after the silane deposition. This indicates that the bis-sulfur silane mostly behaves as a physical barrier. The reduction of anodic current density of AA 2024-T3 by the silane indicates that the anodic dissolution process of the alloy is inhibited by the silane deposition. The reduction in the cathodic current density can be attributable to the geometric effect caused by the silane deposition. That is, the silane deposited on the AA 2024-T3 surface effectively blocks a certain number of active cathodic sites as a result of the formation of AlOSi covalent bonds at the interface. The reduction of the total active surface area results in a decrease in the total cathodic current density.

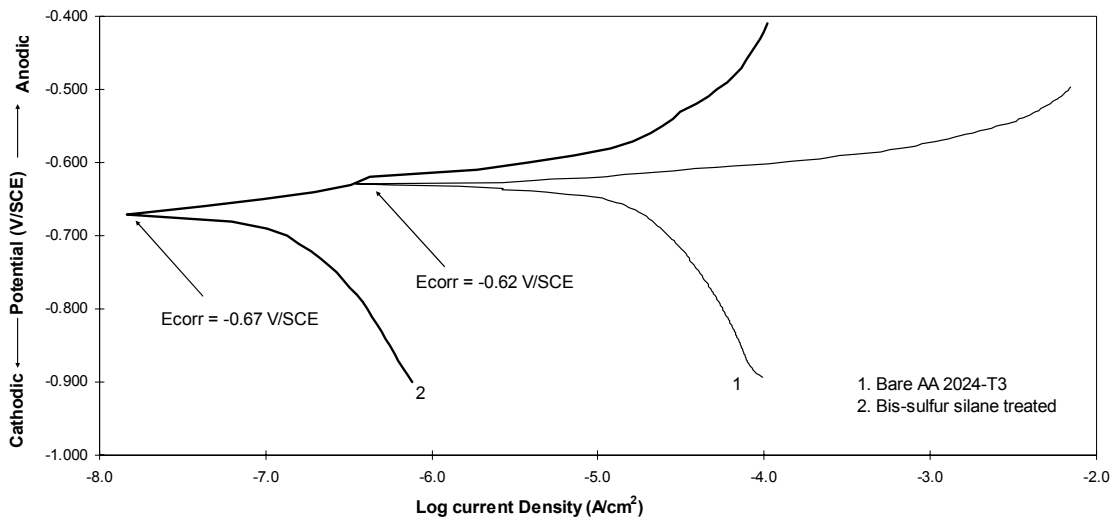


Figure 13. DC polarization curves of AA 2024-T3 treated with and without bis-sulfur silane

EIS was also conducted to monitor the corrosion performance of the bis-sulfur silane-treated AA 2024-T3 system as a function of immersion time in a neutral 0.6M NaCl solution for 30 days [20]. The resistance values of the bis-sulfur silane treated system obtained from the EIS data fitting are shown in Figure 14 as a function of immersion time. Resistance is commonly taken as a measure of corrosion performance of coatings. This is because the resistance is proportional to the porosity of coatings. When immersed in an electrolyte, the coatings soak the electrolyte through the inner pores or free volume. Correspondingly, the resistance of the coatings decreases [23-26].

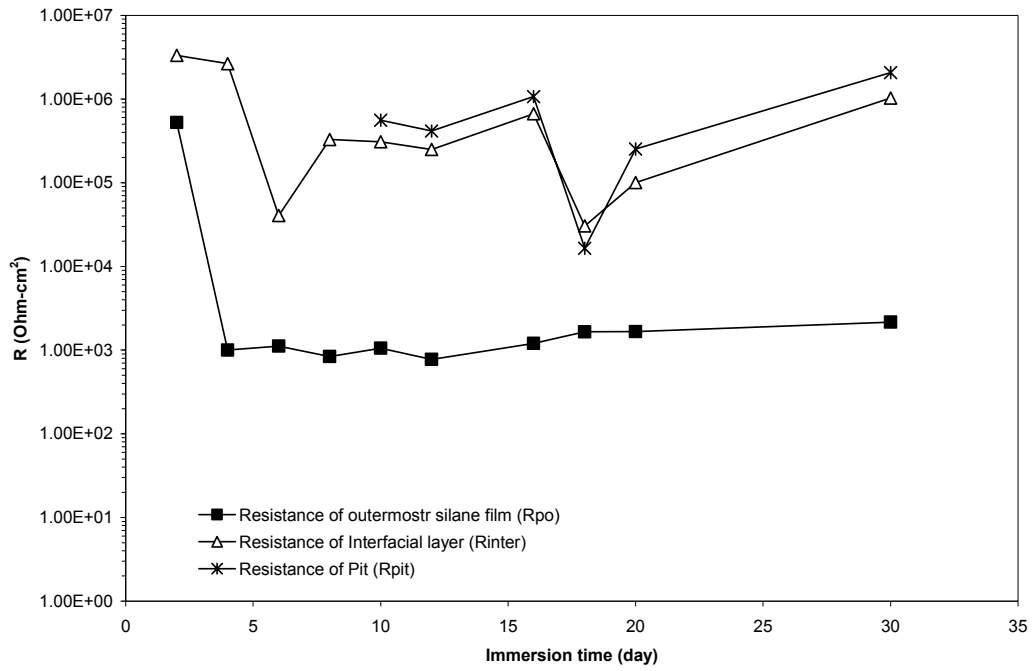
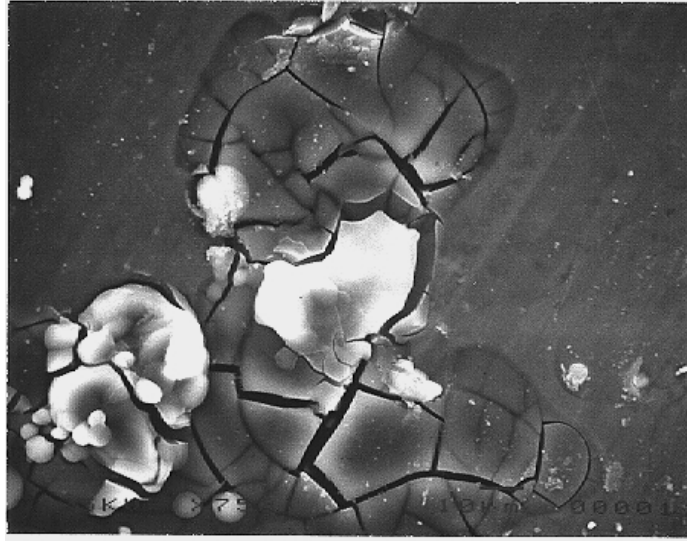


Figure 14. Resistances of silane film, interfacial layer, and pit as a function of time in 0.6M NaCl solution of the bis-sulfur silane treated AA 2024-T3 [20]

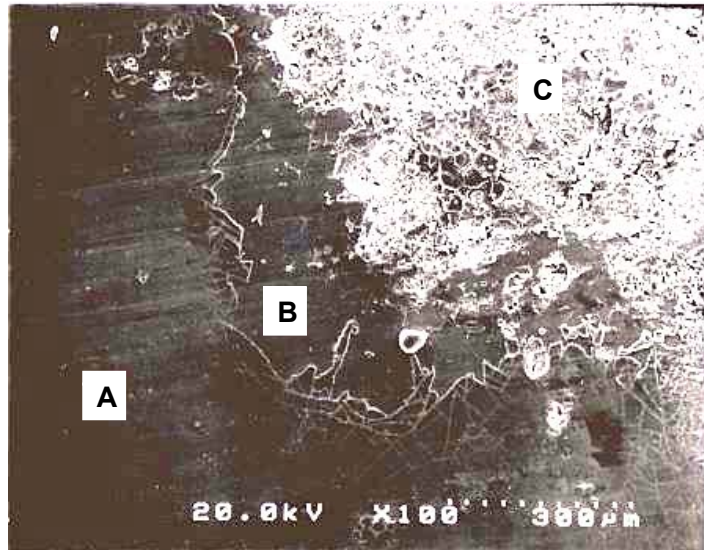
As mentioned earlier, the silane/Al structure consists of three regions. That is, outermost silane film, interfacial layer and the inner Al oxide, as shown in Figure 12. In Figure 14, it is shown that the pore resistance (R_{po}) of the outermost bis-sulfur silane film decreases significantly

after 4 days of immersion, from about $10^6 \Omega\text{-cm}^2$ to $10^3 \Omega\text{-cm}^2$. The value remains constant at around $10^3 \Omega\text{-cm}^2$ afterwards. This indicates that the outermost film has been progressively saturated with the electrolyte within the first 4 days. The resistance of the interfacial layer (R_{inter}) drops by 2 orders of magnitude after 6 days, from $4 \times 10^6 \Omega\text{-cm}^2$ to $4 \times 10^4 \Omega\text{-cm}^2$, and increases again to $5 \times 10^5 \Omega\text{-cm}^2$ after 8 days. The decrease in R_{inter} may reflect the fact that the electrolyte penetrated into the interfacial layer and consequently corrosion occurred in the interfacial region. The corrosion products later on caused “pore blocking” by intruding into the pores in the interfacial layer, leading to the increase in R_{inter} afterwards. After 10 days, a stable pit was observed visually at the surface. The variations in the resistance of the pitted oxide layer (R_{pitt}) are consistent with that of the interfacial layer since then, suggesting that pitting behavior is intimately associated with that of the interfacial layer. In other words, the corrosion activity at the metal surface is greatly affected by the above interfacial layer.

SEM and EDX were performed on the silane-treated alloy surface after immersion of 15 days in the 0.6M NaCl solution (pH 6.5). Two pits were observed at the end of the immersion test. The SEM images of these two pits are shown in Figure 15(a) and (b) [20]. Figure 15(a) shows the morphology of the younger pit, where the silane film starts to crack. In Figure 15(b), the older pit is present with some important morphological features. In general, three different regions indicated as regions A, B and C, are clearly seen in the figure. Region A is the silane film, with some micro-cracks formed in the area adjacent to region B. Region C is the pitting center, where the alloy has been severely eaten away. The corresponding compositions detected by EDX of these three regions are listed in Table 3. The composition of bare AA 2024-T3 is also shown here as a reference [32].



(a)



(b)

Figure 15. SEM image of the pit formed in the bis-sulfur silane treated AA 2024-T3 system after 15 days of immersion in a 0.6M NaCl solution; (a) younger pit and (b) older pit [20]

Table 3. Comparison of chemical compositions (in wt%) of regions A, B and C in Figure 15(b)

| Element | Region A | Region B | Region C | AA 2024-T3 [32] |
|---------|----------|----------|----------|-----------------|
| O | 6.9 | 5.0 | 45.3 | -- |
| Mg | 1.4 | 1.2 | -- | 1.2-1.8 |
| Al | 77.2 | 82.2 | 37.8 | Rem. |
| Si | 5.5 | 3.6 | 1.4 | 0.5 |
| S | 3.9 | 2.1 | 1.6 | -- |
| Cl | -- | 0.3 | 6.2 | -- |
| Cu | 5.1 | 5.9 | 7.6 | 3.8-4.9 |

It is seen in Table 3 that region A contains high amounts of elements Si (5.5 wt%) and S (3.9 wt%). Both are the characteristic elements in the bis-sulfur silane film. It is known that the corrosion of this alloy starts from the dealloying of the active element Mg [33-35], the detection of 1.4 wt% of Mg (i.e., the regular content for AA 2024-T3 alloy) in region A therefore indicates that the AA 2024-T3 substrate is still protected effectively by the silane film in region A.

Region B is the area where part of the silane film has been delaminated. The composition of region B is analogous to that of region A. It should be noted that region B is not simply the bare AA 2024-T3 substrate, as both Si and S detected in region B are not the major alloying elements in AA 2024-T3. The nominal Si content of bare AA 2024-T3 is only 0.5 wt% and no S content is given [32]. The abnormally high amount of Si and S in region B is therefore strong indication that region B is indeed a new region developed in the system, i.e., the interfacial layer illustrated in Figure 12. This interfacial layer is also shown in Figure 11 as an additional time constant (RC3) gradually appearing in the middle of the frequency range. The substrate under the interfacial layer in region B is also protected, as evidenced by the regular amount of Mg (1.2 wt%) detected in this region.

The composition of region C is featured by high contents of O (45.3 wt%) and Cl (6.2 wt%), and low amounts of Al (37.8 wt%). This is indicative of the formation of the corrosion

products, most likely aluminum oxychlorides ($\text{Al}(\text{OH})\text{Cl}_2$ and $\text{Al}(\text{OH})_2\text{Cl}$) [36]. It is also noted in Table 3 that 7.6 wt% of Cu in region C exceeds its regular amount in AA 2024-T3 (i.e., 3.8-4.9 wt%) [32], furthermore, no Mg was detected. This suggests that the corrosion of AA 2024-T3 involves significant dealloying of Mg, which leads to the enrichment of Cu. The amount of Si (1.4 wt%) and S (1.6 wt%) is also noticeable in region C, which stems from the residues of the interfacial layer (shown in region C in Figure 15(b) as small pieces).

From the above corrosion study, it is concluded that rather than the outermost silane film, the crosslinked interfacial layer developed in the system is the major contribution to the corrosion inhibition of AA 2024-T3. The outermost silane film having a large porosity is susceptible to “film-swelling” during immersion, which would easily cause film cracking shown in Figures 15(a) and (b). The interfacial layer, on the other hand, has a small porosity and a good adhesion to the substrate. These two favorable properties would lead to the interfacial layer much more resistant to “film-swelling”, and in the meanwhile would make the corrosion products difficult to transport away from corrosion sites. Since further corrosion or pit growth is under diffusion control [37], the difficulty in the transportation of the corrosion products would inhibit the pit growth and furthermore slow down the entire corrosion process underneath.

It should also be mentioned that the hydrophobic sulfur chains ($-\text{S}_4-$) of the bis-sulfur silane molecule could be another important contributor to the corrosion protection of AA 2024-T3. These sulfur chains entangling with the SiOSi network in both outermost silane film and the interfacial layer would enhance the hydrophobicity of the whole silane system, resulting in retardation of electrolyte intrusion.

4.3. Effect of CH_2 chain length on the corrosion protection of AA 2024-T3

The effect of molecular chain length on the corrosion performance of silane films was studied by using a series of bis-[trialkoxysilyl]alkane silanes and AA 2024-T3 as the substrate.

The bis-[trialkoxysilyl]alkane silanes with various CH₂ chain lengths shown in Table 2 are BTSM, BTSE, BTSH and BTSO. The BTSO molecule is the longest with 8 CH₂ groups, while BTSM is the shortest one with only one CH₂ group. The silane films were deposited on the AA 2024-T3 substrate from their 5% silane solutions (silane/DI water/ethanol = 5/5/90) at pH 4 (adjusted by acetic acid). The as-formed silane films were then characterized using contact angle measurements and EIS in 0.6M NaCl solution (pH 6.5) [38].

Figure 16 shows the low-frequency impedance values at 0.1 Hz (Z_{lf}) of the silane-treated AA 2024-T3 panels after 24 hrs of immersion in the 0.6M NaCl solution and the contact angles for the silane films, as a function of the number of CH₂ groups in the silanes. Z_{lf} values here can be roughly considered as a measure of corrosion performance of silane films [39].

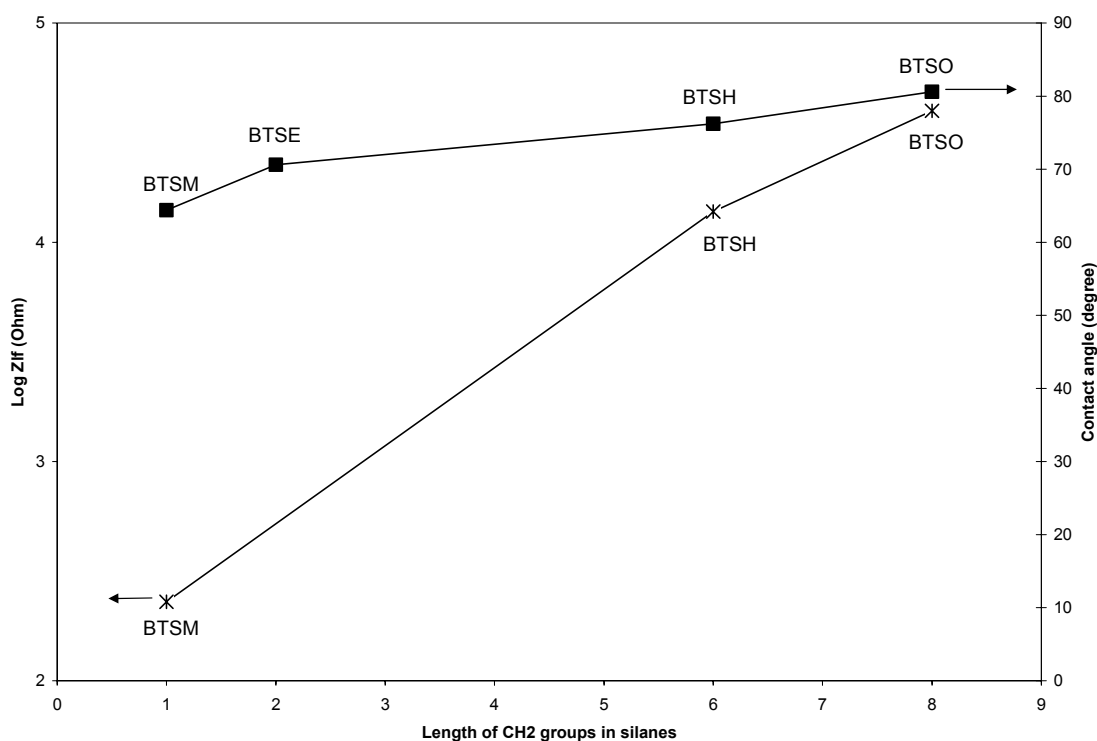


Figure 16. Low frequency impedance and contact angles of bis-[trialkoxysilyl]alkane silanes as a function of length of CH₂ groups [35]

It is observed that the values of both Z_{lf} and contact angles increase with the number of CH_2 groups. The more the number of the CH_2 groups, the longer the chain length, and the higher the values of Z_{lf} and the contact angle. The film with the longest silane molecule, BTSO with 8 CH_2 groups, holds both the highest values of Z_{lf} and contact angle; while BTSM with 1 CH_2 group is the lowest. Apparently, a longer chain length (or the greater number of CH_2 groups) of the silane molecules tends to offer a higher corrosion-resistant silane system. The underlying mechanism may be analogous to that related to the action of the sulfur chain in the bis-sulfur silane mentioned above. Similar to the hydrophobic sulfur chain in the bis-sulfur silane, the CH_2 group is also hydrophobic. The greater the number of CH_2 groups, the longer the molecular chain of bis-[trialkoxysilyl]alkane silanes, and the more hydrophobic the as-formed silane films. Therefore, the most hydrophobic BTSO silane film would retard water ingress as well as corrosive species dissolved in water to intrude into the film, acting similar to the sulfur chain in the bis-sulfur silane film. In considering this hydrophobicity and the good adhesion that the bis-silanes offer, an excellent corrosion protection of AA 2024-T3 can thus be expected after the treatment of BTSO.

5. Thermal stability of silane films

The knowledge of the thermal stability of silane films is of great industrial importance, as the silane films are expected to be used at different temperatures. The thermal stability of free silane films (i.e., without substrates) was investigated using the Thermogravimetric Analysis (TGA) technique. The TGA results for bis-amino and bis-sulfur silanes are shown in Figures 17 (a) and (b). Two small “humps” appear below 200 °C for bis-amino silane in Figure 17 (a), while a more significant change exhibits around 400 °C. The former two “humps” are related to the free water evaporation (< 100°C) and water release in the further crosslinking (< 200°C); whereas the latter dip may be associated with the major decomposition of the silane compounds (<

400°C). The TGA curve of bis-sulfur silane film in Figure 17(b) do not show any changes below 100°C, indicating that the bis-sulfur silane films does not contain a noticeable amount of entrapped free water like the bis-amino silane film does. This further shows that the bis-sulfur silane film is more hydrophobic than the bis-amino silane film. This is understandable as, unlike the bis-amino silane film, the bis-sulfur silane lacks hydrophilic groups such as –NH– groups and thus cannot entrap free water in the film. A tiny hump around 150°C may indicate a further crosslinking in bis-sulfur silane film. Apparently, the degree of crosslinking is small as compared with the bis-amino silane. A major change shown around 300 °C indicates the decomposition of the bis-sulfur silane. Based on the above TGA results, it is concluded that the hydrophilic bis-amino silane has a higher thermal stability than the bis-sulfur silane.

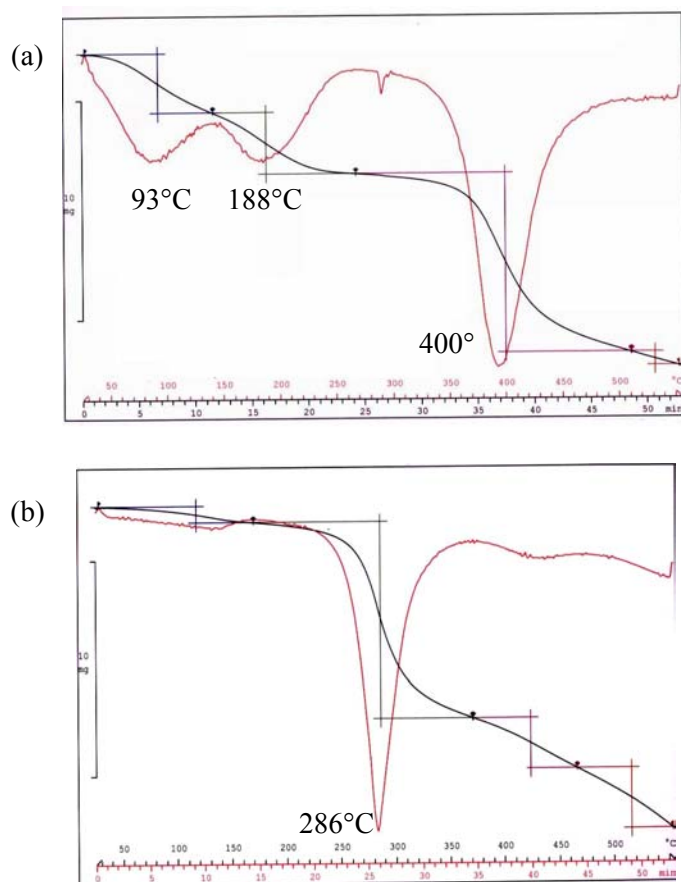


Figure 17. TGA curves of free silane films; (a) bis-amino silane film; (b) bis-sulfur silane film

The CRS panels treated with bis-amino and bis-sulfur silanes were heated up to 200°C for various time periods, i.e., 10 min, 60 min, 120 min, 360 min. DC polarization tests in a 0.6M NaCl solution (pH 6.5) were then conducted in order to evaluate the corrosion performance of the silane films at elevated temperatures. Figure 18 displays corrosion rates (I_{corr}) for the silane-treated CRS panels as a function of curing time. It is clearly seen that I_{corr} for the bis-amino silane-treated CRS remains constant in the curing period (curve 2). In other words, the corrosion performance of the bis-amino silane-treated CRS system is independent of the curing time at 200°C. This confirms that the bis-amino silane film is stable at high temperature, i.e., 200°C. I_{corr} for the bis-sulfur silane-treated CRS, in contrast, gradually increases with increasing curing time at 200°C (curve 3). After only 10 min of curing, the bis-sulfur silane has the value of I_{corr} around 10^{-5} A/cm², lower than that of the bis-amino silane. This suggests that the bis-sulfur silane at this moment still protects the CRS substrate effectively. After 120 min of curing at 200°C, I_{corr} for the bis-sulfur silane-treated CRS increases distinctly, indicating the degradation of the corrosion performance of the bis-sulfur silane. This degradation for the bis-sulfur silane film is apparently associated with its lower decomposition temperature (286°C in Figure 17(b)).

The corrosion behavior of bis-amino and bis-sulfur silane-treated AA 2024-T3 at low temperatures was evaluated using DC polarization tests after cooling at -70°C by using dry ice. The silane-treated AA 2024-T3 panels were cured at 100°C for 10 min and then cooled at -70°C for 2 hrs. After that, DC polarization tests were conducted on these panels. I_{corr} values for the AA 2024-T3 panels treated with and without silanes are compared in Figure 19. In Figure 19, no distinct change is seen for I_{corr} values of the bis-sulfur silane-treated AA 2024-T3 before and after cooling. However, I_{corr} for the bis-amino silane-treated AA 2024-T3 increases about one order of magnitude after cooling. The degradation of the bis-amino silane may be caused by micro-cracking occurring at -70°C, due to its brittle nature. The good performance of the bis-sulfur

silane, on the other hand, implies that this silane film is more flexible than the bis-amino silane film at low temperatures. The micro-cracks are not easily formed in the silane film.

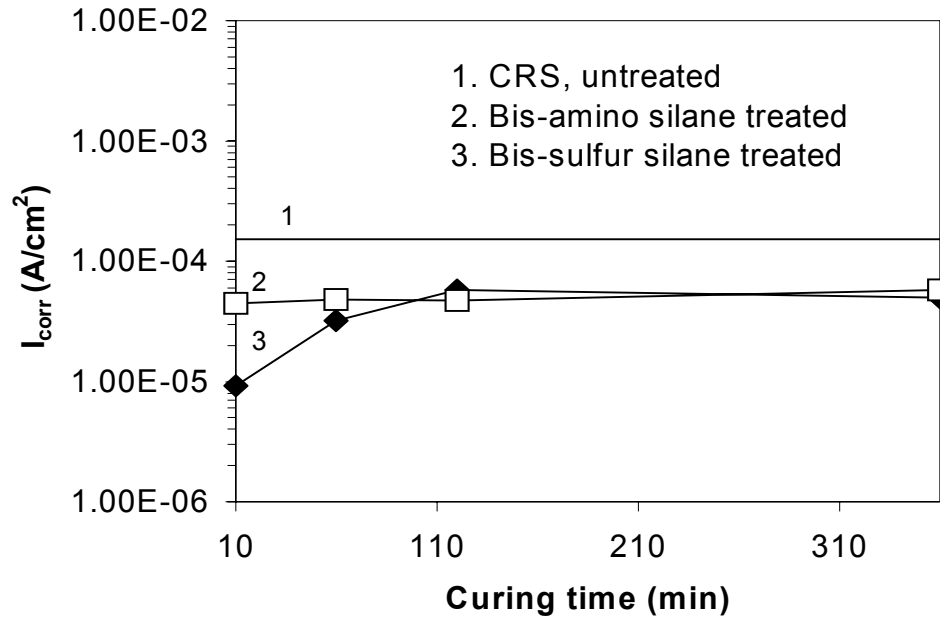


Figure 18. I_{corr} values of silane-treated CRS panels as a function of curing time at 200°C

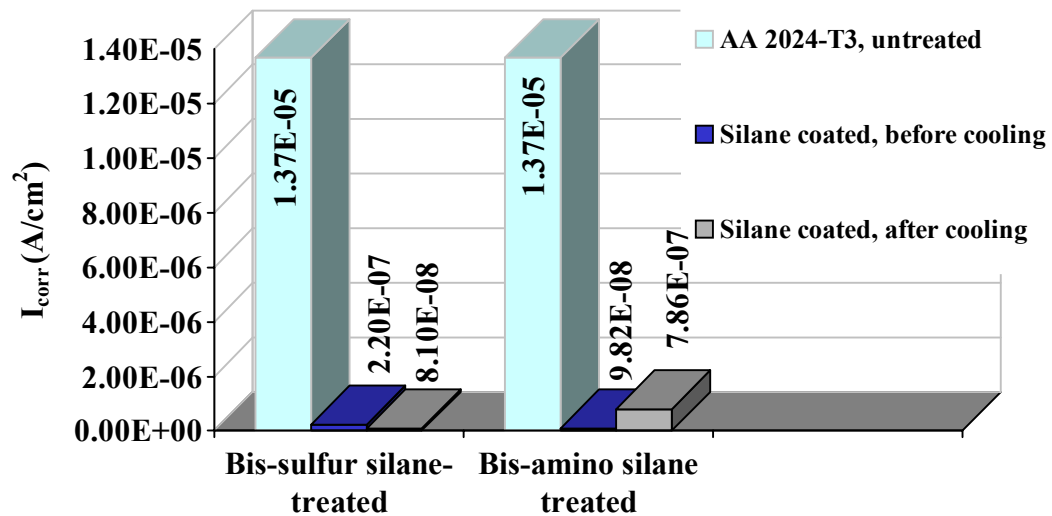


Figure 19. Corrosion rates (I_{corr}) of AA 2024-T3 treated with and without silanes

6. Recent developments in silane processes

In this section, some recent developments in our silane studies are reported. They include nano-structured silane films, “self-healing” silane systems, “super-primers”, and detection of silane films. The studies on understanding the associated mechanisms in these aspects are ongoing.

6.1. Nano-structured silane films

In addition to the anticorrosive efficiency, a major concern of the use of silane films is the mechanical properties of such films. In service, these silane films on metals should be capable of resisting mechanical damages by impact, scratch and wear. Therefore, one of our current research subjects is to improve mechanical properties of silane films by loading nano-particles into the films.

Silica nano-particles were added into 5% bis-sulfur silane solutions according to the following 2-step procedure. First, different amounts of silica nano-particles, i.e., 0.01%, 0.03%, 0.04% and 0.1% (in weight percent) were mixed with DI water using a high-speed blender until uniform silica colloidal solutions were obtained. The estimated mixing time was around 20 min. 5 parts of the silica colloidal solutions were then added into the silane/ethanol mixture at the mixing ratio of 5/90 (v/v). The percents of silica nano-particles in the silane solutions then became 5 ppm, 15 ppm, 20 ppm and 50 ppm.

The values of E_{corr} and corrosion rates (I_{corr}) of nano-structured bis-sulfur silane treated AA 2024-T3 systems are plotted as a function of the contents of silica particles in the corresponding silane solutions in Figure 20 [40]. A dip in E_{corr} is seen for the film obtained from the 5 ppm silica-containing silane solution, shifting from -0.63 V/SCE to -1.0 V/SCE. This indicates that the silane film from the 5 ppm silica-containing silane solution behaves as a

cathodic barrier like cerium compounds [41–43]. Such nano-structured films somehow retard the cathodic reactions, and therefore inhibit the entire corrosion process in the system. Such cathodic inhibitive behavior disappears with an increase in silica content up to 15 ppm, inferring that the bis-sulfur silane film no longer performs as a cathodic inhibitive layer when the silica amount in the film exceeds a certain value.

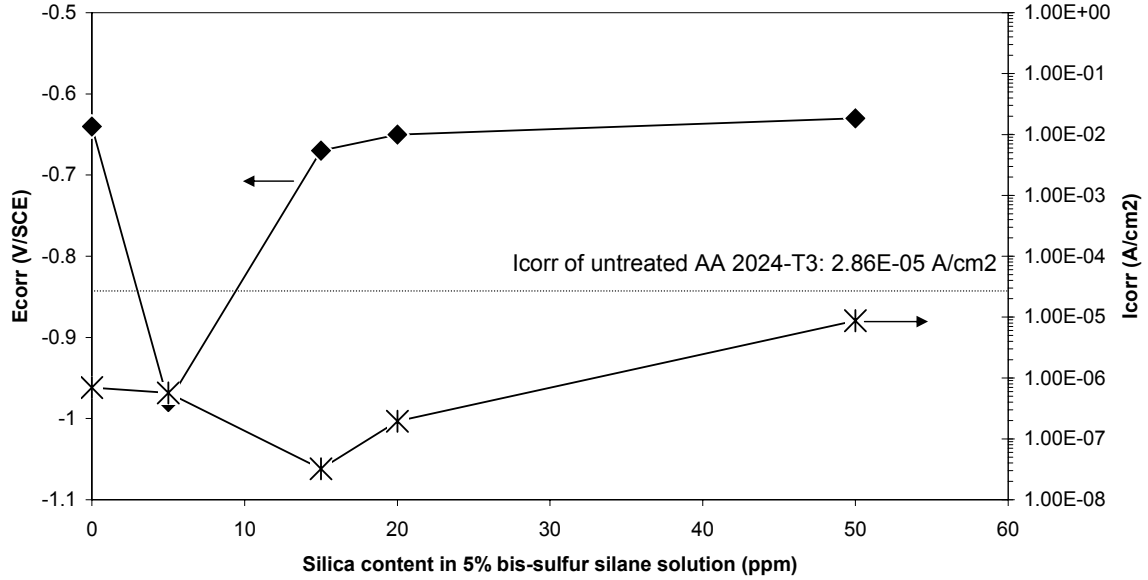


Figure 20. E_{corr} and I_{corr} of bis-sulfur silane treated AA 2024-T3 systems as a function of silica content in the film [40]

The trend in the I_{corr} values with increasing in silica contents in the corresponding silane solutions is also shown in Figure 20. A drop in I_{corr} is observed corresponding to the silica content of 15 ppm in the solution. The I_{corr} values, however, shift back when further increasing the silica content in the solution. At the silica content of 50 ppm, the I_{corr} value for the corresponding silane film exceeds that of the unloaded bis-sulfur silane film and gradually approaches the I_{corr} value for the untreated AA 2024-T3, showing that the corrosion inhibition of the silane film degrades when loaded with too many silica particles.

On the basis of the above results, it can be generally concluded that a small amount of silica nano-particles (e.g., obtained from the silane solution with silica ≤ 15 ppm) does improve the corrosion performance of the bis-sulfur silane film on AA 2024-T3. However, such improvement diminishes when further increasing the silica amount in the film (e.g., silica in the solution > 15 ppm). Moreover, an extra large amount of silica particles in the film even degrades the corrosion performance of the silane film (e.g., > 50 ppm) and causes premature film delamination. A proposed mechanism is given in [40].

The values of hardness of the bis-sulfur silane films loaded with and without silica nano-particles are shown in Figures 21 [40]. It is seen that the hardness values for the silane films obtained from the 50 ppm silica-containing silane solution improve to some extent as compared to the film without silica particles. This confirms that the silane film can be hardened by the loading of silica nano-particles as is expected.

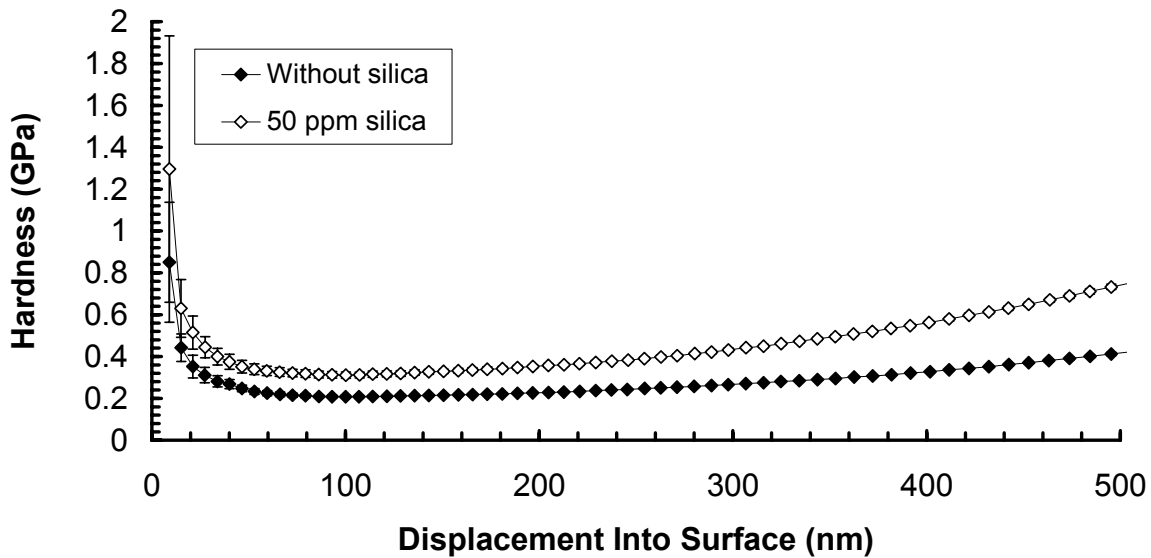


Figure 21. Hardness of bis-sulfur silane films loaded with and without silica nano-particles, as a function of displacement into the metal surface [40]

6.2. “Super-primers” systems

Water-based silanes were mixed with primer resins. With the development of these silane-containing resin systems (or “super-primers”), it is hoped to further enhance both corrosion protection and paint adhesion of metals. Figure 22 gives the EIS results for one super-primer applied on hot-dipped galvanized steel (HDG) panels. It is seen that although the silane X-treated HDG initially has the highest impedance value, it decreases significantly after 3 days of immersion in a 0.6 M NaCl solution. The impedance for the “super-primer” treated HDG, on the other hand, does not vary much with immersion time. This indicates that this “super-primer” system indeed strengthened corrosion resistance of HDG, as compared with the silane film alone.

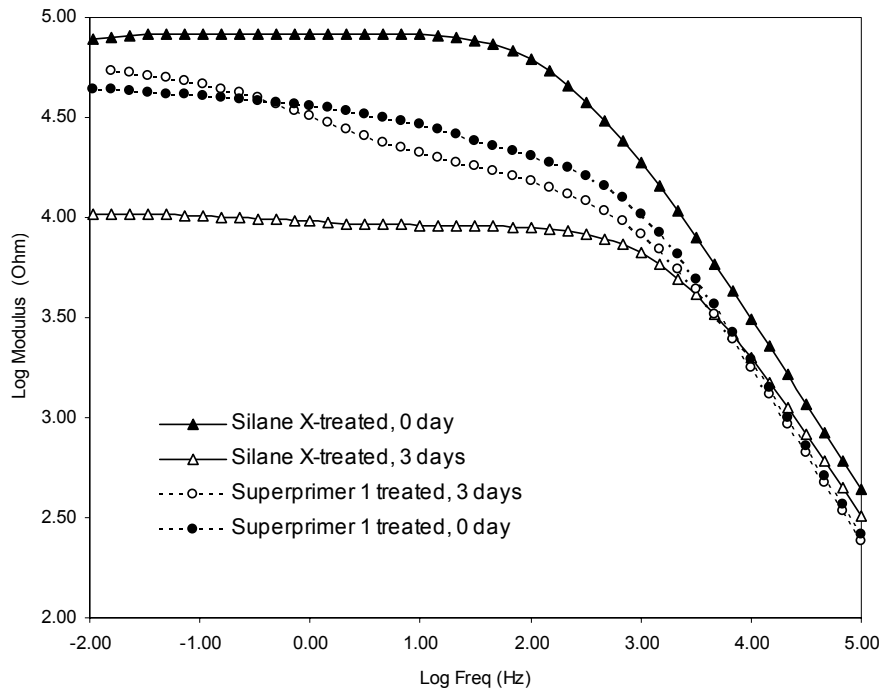


Figure 22. EIS plots of HDG treated with Superprimer 1 and Silane X

6.3. “Self-healing” silane systems

When a chromated metal surface has damaged locally such as scratches or pinpoints, the chromium ions are capable of diffusing to the damaged areas, reforming a protective layer in situ

[44,45]. Hence, the further corrosion at the damage places is well prevented. This action is called “self-healing” effect. Unfortunately, a crosslinked silane film does not exhibit such healing effect.

In a recent project, a trace amount of environmentally-friendly corrosion inhibitors such as cerium compounds was incorporated into silane solutions, in the hope of developing “self-healing” silane systems. After doping a small amount of corrosion inhibitors, the resulting silane films were surprisingly found to possess a satisfactory “self-healing” effect. An example is shown in Figure 23, where the bis-sulfur silane treated AA 2024-T3 panels with bis-sulfur and without cerium ions (Ce^{3+}) have been exposed to a 0.6 M NaCl solution (pH 6.5) for 7 days. Both panel surfaces were cross-scribed before testing. In Figure 23(a), corrosion is obvious along the scribe line although the other area has been well-protected by the silane film. After incorporation with Ce^{3+} ions (i.e., 1000 ppm in the corresponding silane solution), the resulting Ce^{3+} -loaded bis-sulfur silane film shown in Figure 23(b) protects the whole surface (the scribe lines as well as the intact area) very well without showing corrosion at all. In the former case, most SiOH groups are consumed during the curing process, forming a crosslinked structure. Even if there are a small number of un-used SiOH left in the crosslinked film, these SiOH groups are still hard to move due to a high degree of the chain entanglement. Consequently, “self-healing” effect is not expected. In the latter case, the Ce^{3+} ions loaded in the silane film are small in volume, and therefore can move freely within the film once dissolved in water. Once local damages occur, those Ce^{3+} ions readily diffuse to the places in an aqueous environment and “cure” the “damaged” metal by forming protective Ce^{3+} compounds in situ [43].

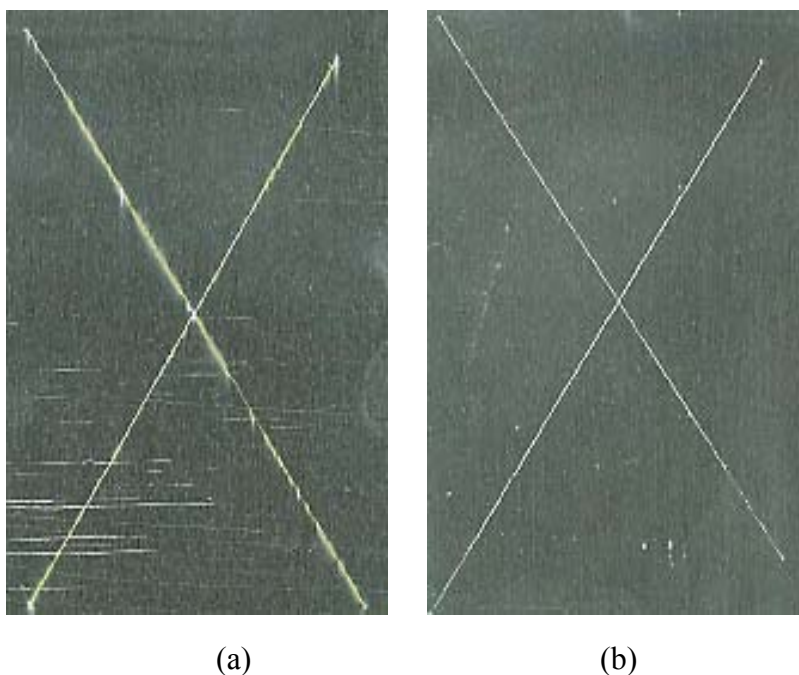


Figure 23. AA 2024-T3 panels treated with bis-sulfur silane (a) and bis-sulfur silane loaded with Ce^{3+} ions (b), after 7 days of immersion in a 0.6 M NaCl solution (pH 6.5)

6.4. *Detection of silane film on metals by colorants*

Unlike chromate films which can be easily identified by their intrinsic yellow color, silane films are transparent and colorless. Thereby, detection methods are desirable in order to realize in-line control of silane films in industry. The colorants that we have tested fall into two major catalogues: dyes and color nano-particles. Desirable colorants should meet the following requirements. (1) Intensive coloring ability which should give the ultrathin silane film (100 to 400 nm) a noticeable color. (2) No negative impacts on the corrosion performance of silane films. (3) No negative impacts on the paint adhesion of silane films. On this basis, a number of colorants have been screened. Now it is safe to say that we have found at least one colorant which meets all the above requirements very well. Figure 24 compares the corrosion performance of the bis-sulfur silane films deposited on AA 2024-T3 with and without dyeing. It is clearly seen that there is no

difference between the panels with and without colorant 1, suggesting that the addition of colorants does not have negative effect on the corrosion protection of the silane-treated metal.

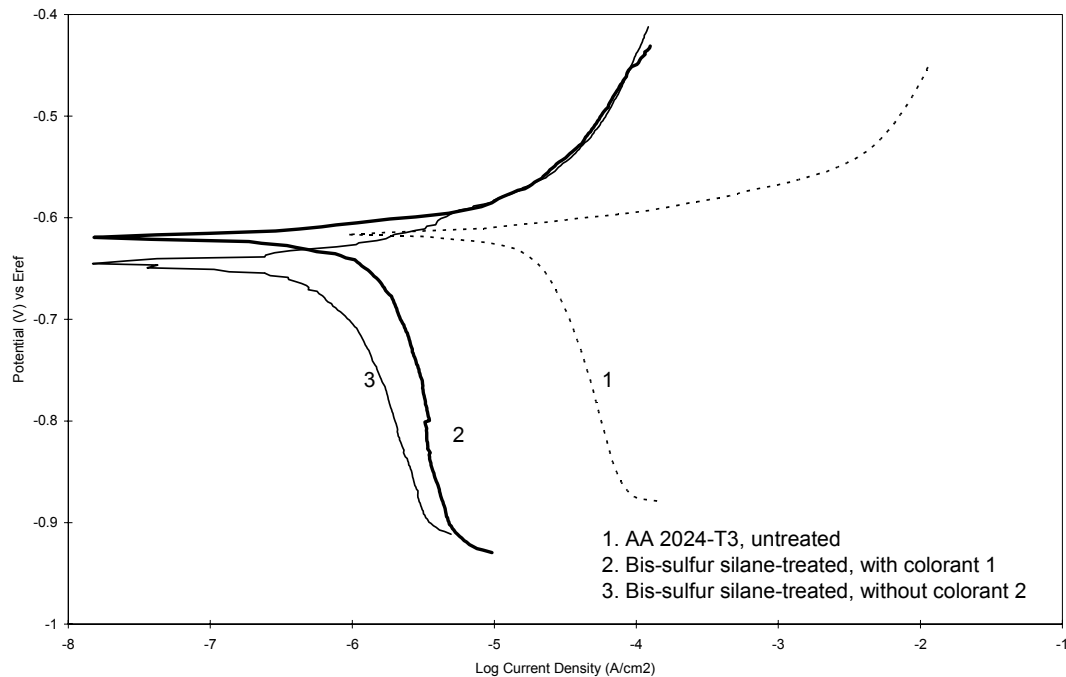


Figure 24. DC polarization curves of bis-sulfur silane-treated AA 2024-T3 with and without dying

Acknowledgements

The authors gratefully acknowledge the financial support for this work by the Air Force Office of Scientific Research under contract F49620-01-1-0352 and by Chemat Inc..

References

1. W. J. van Ooij and T. F. Child. CHEMTECH, 28, (1998) 26
2. V. Subramanian and W. J. van Ooij, CORROSION, 54, 204(1998)

3. V. Subramanian, Ph. D. Dissertation, University of Cincinnati, Department of Materials Science and Engineering, 1999.
4. G. P. Sundararajan, M. S. Thesis, University of Cincinnati, Department of Materials Science and Engineering, 2000.
5. W. J. van Ooij, D. Zhu, G. P. Sundararajan, S. K. Jayaseelan, Y. Fu and N. Teredesai. *Surf. Engg.* 16, (2000) 386
6. W. J. van Ooij and D. Zhu, *CORROSION*, 157(5), (2001) 413
7. M. A. Petrunin, A. P. Nazarov, and Yu. N. Mikhailovski, *J. Electrochem. Soc.* 143, (1996) 251
8. A. M. Beccaria and L. Chiaruttini, *Corros. Sci.*, 41, (1999) 885
9. P. R. Underhill and D. L. Duquesnay, Corrosion resistance imparted to aluminum by silane coupling agents, in: K. L. Mittal (Ed.), *Silanes and Other Coupling Agents Vol. 2*, K. L. Mittal Ed., VSP, Utrecht, (2000) 149
10. Z. Pu, W. J. van Ooij and J. E. Mark, *J. Adhes. Sci. Technol.*, 11 (1997) 29
11. W. J. van Ooij and A. Sabata, *J. Adhes. Sci. Technol.*, 5, (1991) 843
12. C. Zhang, Ph. D. Dissertation, University of Cincinnati, Department of Materials Science and Engineering, 1997
13. S. E. Hörnström, J. Karlsson, W. J. van Ooij, N. Tang and H. Klang, *J. Adhes. Sci. Technol.*, 10, (1996) 883
14. W. Yuan and W. J. van Ooij, *J. Colloid Interface Sci.*, 185, (1997) 197
15. J. Song and W. J. van Ooij, *ATB Metallurgie*, 37, (1997) 137
16. D. Zhu and W. J. van Ooij, *J. Adhesion Sci. Technol*, 16(1), (2002) 1235
17. E. P. Plueddemann, *Silane Coupling Agents*, 2nd ed., Plenum Press, New York, 1991.
18. K. L. Mittal (Ed.), *Silanes and Other Coupling Agents*, VSP, Utrecht, (1992)
19. K. L. Mittal (Ed.), *Silanes and Other Coupling Agents*, Vol. 2, VSP, Utrecht, (2000)
20. D. Zhu and W. J. van Ooij, *Corros. Sci.*, accepted, 2002

21. D. Zhu, Ph. D. Dissertation, University of Cincinnati, Department of Materials Science and Engineering, in press, 2002.
22. F. D. Osterholtz and E. R. Pohl, J. Adhesion Sci. Technol., 6, (1992) 127
23. S.F. Mertens, C. Xhoffer, B.C. Cooman and E. Temmerman, CORROSION, 53, 381 (1993)
24. F. Mansfeld, J. Appl. Electrochem., 25, 187 (1995)
25. M. Kendig and J. Scully, Corrosion, 46, 23 (1990)
26. H.P. Hack and J.R. Scully, J. Electrochem. Soc., 138, 33 (1991)
27. R.F. Allen and N.C. Baldini, editors, "1998 ASTM Annual Book of ASTM Standards", ASTM, West Conshohocken, Pennsylvania, (1998)
28. G. Socrates, "Infrared Characteristic Group Frequencies", John Wiley & Sons, New York, 1994.
29. K. P. Battjes, A. M. Barolo and P. Dreyfuss, J. Adhesion Sci. Technol., 5, 177 (1991)
30. F. J. Boerio, and J. W. Williams, Proc. 36th Annu. Conf. Reinforced Plastics/Composites, Inst., Sect. 2-F (1981)
31. S. R. Culler, M. S. Thesis, Case Western Reserve University, Cleveland, OH (1982)
32. D. A. Jones, "Principles and Prevention of Corrosion", 2nd ed., Prentice-Hall Inc, (1996) 556
33. R. G. Buchheit, R. P. Grant P. F. Hlava, B. McKenzie, and G. L. Zender, J. Electrochem. Soc., 144 (8), (1997) 2621
34. C. Blanc, B. Lavelle, and G. Mankowski, Corr. Sci., 41 (1999) 421
35. G. S. Chen, M. Gao, and R. P. Wei, Corrosion, 52(1), (1996)
36. K. P. Wong, R. C. Alkire, J. Electrochem. Soc, 129, (1982) 464
37. G. S. Frankel, L. Stockert, F. Humkeler, H. Bohni, CORROSION, 43, (1987) 429
38. A. Lamar and D. Zhu, 'Corrosion protection of AA 2024-T3 by bis-nonfunctional silanes', *in the proceeding of '2002 Tri-service Corrosion Conference*, sponsored by the Air Force Office of Scientific Research, held January 14-18, San Antonio, TX, 2002
39. J. A. Grandle and S. R. Taylor, Corrosion, 50, (1994) 792

40. V. Palanivel, D. Zhu and W. J. van Ooij, presented at “The Workshop on Nanoscale Approaches to Multifunctional Coatings”, Keystone, CO, August 12-16, 2002
41. Parkhill, R. L., Knobbe, E.T. and Donley, M.S., Progress in Organic Coatings, 41(4), (2001) 261
42. Morris, E., Stoffer, J.O., O'Keefe, T.J., Yu, P., and Lin, X., Polym. Mater. Sci. Eng., 81, (1999) 167
43. M. A. Arenas, M. Bethencourt, F. J. Botana, J. de. Damborenea and M. Marcos, Corros. Sci., 43, (2001) 157
44. M.W. Kendig, A. J. Davenport, H. S. Isaacs, Corros. Sci., 34, (1993) 41
45. H. A. Katzman, G. M. Malouf. R. Bauer, G. W. Stupian, Appl. Surf. Sci., 2, (1979) 416